ARTICLES
https://doi.org/10.1038/s41593-018-0153-x
nature neuroscience

A neural network for intermale aggression to establish social hierarchy

Stefanos Stagkourakis*, Giada Spigolon, Paul Williams, Jil Protzmann, Gilberto Fisone and Christian Broberger*

Intermale aggression is used to establish social rank. Several neuronal populations have been implicated in aggression, but the circuit mechanisms that shape this innate behavior and coordinate its different components (including attack execution and reward) remain elusive. We show that dopamine transporter-expressing neurons in the hypothalamic ventral premammillary nucleus (PMv^{DAT} neurons) organize goal-oriented aggression in male mice. Activation of PMv^{DAT} neurons triggers attack behavior; silencing these neurons interrupts attacks. Regenerative PMv^{DAT} membrane conductances interacting with recurrent and reciprocal excitation explain how a brief trigger can elicit a long-lasting response (hysteresis). PMv^{DAT} projections to the ventrolateral part of the ventromedial hypothalamic and the supramammillary nuclei control attack execution and aggression reward, respectively. Brief manipulation of PMv^{DAT} activity switched the dominance relationship between males, an effect persisting for weeks. These results identify a network structure anchored in PMv^{DAT} neurons that organizes aggressive behavior and, as a consequence, determines intermale hierarchy.

Aggression is a pervasive, innate social behavior, most commonly displayed in the interactions between males of the same species[1], while female aggression is rarer and typically expressed in the protection of offspring[1,2]. Rodent intermale aggressive behavior follows a stereotyped escalating pattern that ceases once one combatant assumes a submissive posture[3]. Thus, rather than aiming to inflict physical injury, typical intermale aggression serves to establish interindividual hierarchy and is integral to determining social rank and construct societal structure. When physiological aggression goes beyond its normal boundaries, such as in pathological forms of violence[4], societal structure is threatened.

Early studies in cat[5] and rodents[6] identified a hypothalamic rostrocaudal column designated the 'hypothalamic attack area', which, when stimulated, elicits attack[6,7]. Subsequent investigations have revealed a number of nuclei involved in aggression, including the ventrolateral subdivision of the ventromedial hypothalamic nucleus (VMHvl)[8], the lateral septum[9], basal forebrain[10], and medial amygdala[11]. While these structures mediate acute attack behavior, few if any have been implicated in the physiological function of intermale aggression: the establishment of interindividual hierarchy. Furthermore, the circuit structure and properties underlying aggression remain elusive. Current understanding of the underlying neuronal substrates is insufficient to explain the salient features of this behavior, such as its persistence upon removal of the stimulus that triggered it (hysteresis)[12,13]. Similarly, while aggression has been associated with rewarding properties[10], the network underlying this feature is largely unknown. Here we addressed how a neuronal circuit that generates and coordinates the behavioral components of aggression is organized and how this circuit's activity translates to the establishment of interindividual hierarchy.

We focused on the hypothalamic ventral premammillary nucleus (PMv), a nucleus that has been implicated in reproductive maturation[14], as well as in aspects of social behaviors such as close investigation, mating, and intermale and maternal aggression[15–19]. Notably, the PMv is reciprocally connected to several of the other nuclei within the hypothalamic attack area[20,21], suggesting that it may play a central role in aggressive behavior. Neurons in this nucleus are virtually exclusively glutamatergic[22], including a subset of neurons also expressing the dopamine transporter (DAT)[23] (Supplementary Fig. 1d–g) that are unlikely to be dopaminergic, as (for example) they do not contain tyrosine hydroxylase[18]. Here we used DAT-Cre mice to genetically tag these glutamatergic neurons (PMv^{DAT}) and investigate their properties and role in aggression.

Results

PMv^{DAT} neuron activity during aggression. DAT$^+$ neurons make up 34% of PMv neurons and are evenly distributed throughout the nucleus (Fig. 1a–c and Supplementary Fig. 1a–c). We first addressed whether PMv^{DAT} neuron activity is related to aggressive behavior and aggression phenotype. Male mice were screened for aggressive behavior in the resident–intruder (RI) assay[24]: 77% of all residents were aggressors (AGGs) and 23% were nonaggressors (NONs; Fig. 1d). Repeated daily RI tests increased aggressiveness in the AGGs but did not change the phenotype of NONs (Fig. 1e,f). We next compared brain activation patterns of AGGs versus NONs using the immediate early gene product c-Fos[25,26], which is induced in the PMv after exposure to conflict[16–18]. After RI testing (Supplementary Fig. 1h), PMv neurons were significantly more activated in AGGs than in NONs (Fig. 1g,h and Supplementary Fig. 1i–q), while in AGGs exposed to intruder bedding (odor), there was a mild increase (Fig. 1h). In AGGs, attack duration was correlated to the proportion of c-Fos$^+$DAT$^+$ co-localizing neurons (Fig. 1i), but not to the total number of c-Fos$^+$ neurons in the PMv (Supplementary Fig. 1r), specifically associating PMv^{DAT} neurons with activation during aggression. We also observed an activation of the PMv^{DAT} cells in the intruder ($44.82 \pm 12.43\%$ of DAT$^+$ cells immunoreactive for c-Fos; not shown), in agreement with a recent report[18]. To address whether the excitability of PMv^{DAT} neurons in residents differs depending on phenotype, neuronal activity was investigated through whole-cell patch-clamp recordings of hypothalamic slices from AGGs and NONs. PMv^{DAT} neurons from AGGs typically discharged tonically, whereas in NONs these neurons

Department of Neuroscience, Karolinska Institutet, Stockholm, Sweden. *e-mail: stefanos.stagkourakis@ki.se; christian.broberger@ki.se

were typically quiescent, correlating with more depolarized and hyperpolarized membrane potentials, respectively (Fig. 1j–l). These experiments show that the activity of PMv^{DAT} neurons was tightly correlated to intermale aggression. To investigate a causal role, we next performed in vivo optogenetic studies.

Activation and silencing of PMv^{DAT} neurons. Parameters for channelrhodopsin-2 (ChR2)-mediated excitation and halorhodopsin (eNpHR3)-mediated inhibition were first verified and optimized, including 20-Hz, 5-ms pulses that induced optimal spike fidelity in vitro (Supplementary Fig. 2a–g) and robust c-Fos activation of PMv^{DAT} neurons in vivo (Supplementary Fig. 2h–n). Cre-dependent expression of the injected constructs was induced in the majority of PMv^{DAT} cells (Supplementary Fig. 2o,p), while injection of the eYFP and rhodopsin-eYFP AAVs in the PMv of wild-type mice did not yield eYFP expression ($n=12$; data not shown). Both AGGs and NONs were subjected to ChR2 stimulation in vivo (Fig. 2a,b). Castrated or ovariectomized C57BL/6J and BALB/c mice, which did not trigger attack behavior in the resident under control conditions[13] (Fig. 2c), were used as intruders. Low-intensity PMv^{DAT} neuron optogenetic stimulation in AGGs increased the duration of close investigation, while higher-intensity levels elicited attack behavior (Fig. 2c,g). Both attack probability and intensity were increased in response to high-intensity stimulation in AGGs, with 86% of trials evoking attack behavior with similar attack bout duration in response to castrated ($n=58$) and ovariectomized intruders ($n=23$; Fig. 2d–f and Supplementary Videos 1 and 2). Notably, the lag from light-onset to start of attack was significantly briefer than the lag from light-termination to end of attack (Fig. 2e). Often, brief (<20 s) ChR2 stimulation induced long attack episodes lasting over several minutes, indicative of a striking hysteresis effect. PMv^{DAT} stimulation in AGGs did not, however, evoke attack against inanimate objects in repeated trials (Supplementary Fig. 3a–d). In NONs, ChR2 stimulation of PMv^{DAT} neurons evoked an intensity-dependent increase in close investigation duration but no escalation to aggression (Fig. 2h–j).

To test the effect of acute silencing of PMv^{DAT} neurons in intermale aggressive behavior, we performed in vivo eNpHR3 stimulation in AGGs, using intact male intruders, a setup with high levels of baseline aggression in the RI test (Fig. 2k,l). Optogenetic silencing of PMv^{DAT} neurons in residents during charging (i.e., assuming body position with access to the intruder's back) impeded the naturally occurring transition to attack (Fig. 2m,n). eNpHR3 stimulation during an ongoing attack ended the attack, reducing average attack bout duration (Fig. 2m,o,p and Supplementary Video 3). To examine the effects of chronic ablation of PMv^{DAT} neurons on aggressive behavior in AGGs, we stereotactically introduced Cre-dependent diphtheria toxin A subunit, resulting in an average loss of 77% of the PMv^{DAT} cells (Supplementary Fig. 4a–d). In contrast, the sizes of DAT^{+} populations 'flanking' the PMv injection site (midbrain and arcuate dopamine neurons) were not affected (Supplementary Fig. 4e–j), suggesting a PMv-restricted lesion. In PMv^{DAT}-ablated AGG residents, aggression (including intensity, quantified as attack duration; probability, as evidenced in latency to first attack; and attack frequency versus remaining number of PMv^{DAT} cells) was markedly reduced in the RI test (Supplementary Fig. 4k,l,n), yet mating behavior was not disturbed (Supplementary Fig. 4o–q). These results suggest that PMv^{DAT} neuron activity is necessary and sufficient for the expression of aggressive behavior.

Mechanisms for reverberation of neuronal activity in PMv. A striking observation in the optogenetic experiments in AGGs during RI testing was the persistence of attack behavior outlasting the ChR2 stimulation (Fig. 2c,e). Hysteresis is a common attribute of emotional states including aggression[12,13,27], yet little is known about the underlying neural mechanisms. The PMv^{DAT} neurons were investigated in vitro for features that could explain how a transient trigger may result in enduring circuit activation.

In PMv^{DAT} whole-cell recordings, brief (0.5 s) positive current pulses were followed by long-lasting (~18 s) repetitive bursting, a phenomenon that persisted in the presence of tetrodotoxin (TTX; Fig. 3a). Similarly, optogenetic pulses (3-s duration, 5 Hz, 5 ms) also evoked repetitive firing (Supplementary Fig. 5n–p). Brief (1 s) negative current pulses resulted in an oscillatory postinhibitory rebound (PIR), similarly followed by regenerative bursting, which in the presence of TTX took the shape of a prolonged plateau potential (Fig. 3b). Negative current pulses revealed a depolarizing 'sag' (indicative of the hyperpolarization-activated cation current, I_h, a common feature of rhythmogenic cells), followed by a PIR (Fig. 3b and Supplementary Fig. 6a). Application of an I_h antagonist, ZD-7288, abolished the sag, and co-application of ML-218, a selective T-type low-voltage activated Ca^{2+} current antagonist, abolished the PIR (Supplementary Fig. 6a) and the repetitive bursting after brief stimulation (not shown). PMv^{DAT} neurons thus have a capacity for both excitation- and inhibition-triggered reverberatory discharge, likely mediated by a cyclical interaction of I_h and I_T, similar to the neuronal architecture of for example, the thalamus[28].

To explore whether intranuclear interconnectivity can provide a source of excitation to trigger repetitive bursting, we performed paired whole-cell recordings of PMv^{DAT} neurons. Reciprocal synaptic connectivity was commonly observed ($n=5$ of 11 pairs). Evoked action potentials reliably elicited brief-latency excitatory postsynaptic potentials blocked by the AMPA and NMDA glutamate receptor antagonists CNQX and AP5 (Fig. 3c–e). Reconstruction of synaptically connected PMv^{DAT} neuron pairs revealed closely apposed cell processes indicative of interconnectivity (Fig. 3f). Individual reconstructed PMv^{DAT} neurons exhibited extensive arborization within the PMv borders, enveloping several other neighboring PMv^{DAT} neurons (Supplementary Fig. 6b–j). Lastly, PMv^{DAT} neuron contralateral projections were observed[20] (Supplementary Fig. 6k,l); these could synchronize and sustain reverberatory activity in PMv nuclei between hemispheres.

Optogenetic experiments provided further evidence for recurrent synaptic excitation among PMv^{DAT} cells. The compound depolarization that follows a light-evoked action potential in ChR2-eYFP-expressing PMv^{DAT} neurons (Supplementary Fig. 5a,b) was unaffected by blockade of $GABA_A$ receptors (with gabazine) or polysynaptic relay (with TTX and 4AP), but diminished in amplitude and time constant under glutamate receptor blockade (CNQX and AP5; Supplementary Fig. 5b,c). Following brief (20 Hz, 5 ms; 500-ms duration) optogenetic train stimulation, excitatory postsynaptic currents increased in frequency and amplitude 10 s post-stimulation, suggestive of interconnectivity and reverberation of activity within PMv (Supplementary Fig. 5e–j). PMv^{DAT} neurons also formed excitatory monosynaptic contacts with DAT^{-} PMv neurons (Supplementary Fig. 5k–m).

The VMHvl is a nucleus of key importance in social behaviors, including attack behavior[13,16,29,30], and is a target of projections from the PMv[18]. Antero- and retrograde tracing demonstrated that PMv^{DAT} neurons are a source of innervation of the VMHvl (Supplementary Fig. 7a–c,h–k). By performing in vitro functional connectivity experiments, we found that the majority of recorded and reconstructed VMHvl neurons receive strong monosynaptic glutamatergic input from PMv^{DAT} neurons (Fig. 3g–i and Supplementary Fig. 8a–g). VMHvl neurons expressing estrogen receptor-α, which comprise a VMHvl subpopulation specifically implicated in intermale social behavior[13], are surrounded by dense PMv^{DAT} neuron fibers (Supplementary Fig. 8h,i). Furthermore, VMHvl neurons receiving input from PMv^{DAT} cells were found to project back to the PMv (Fig. 3j–l), suggesting a feedforward excitation loop, since the majority of VMHvl neurons are glutamatergic[22,31]. Lastly, ChR2-mediated stimulation of PMv^{DAT} neuron terminals evoked multiple

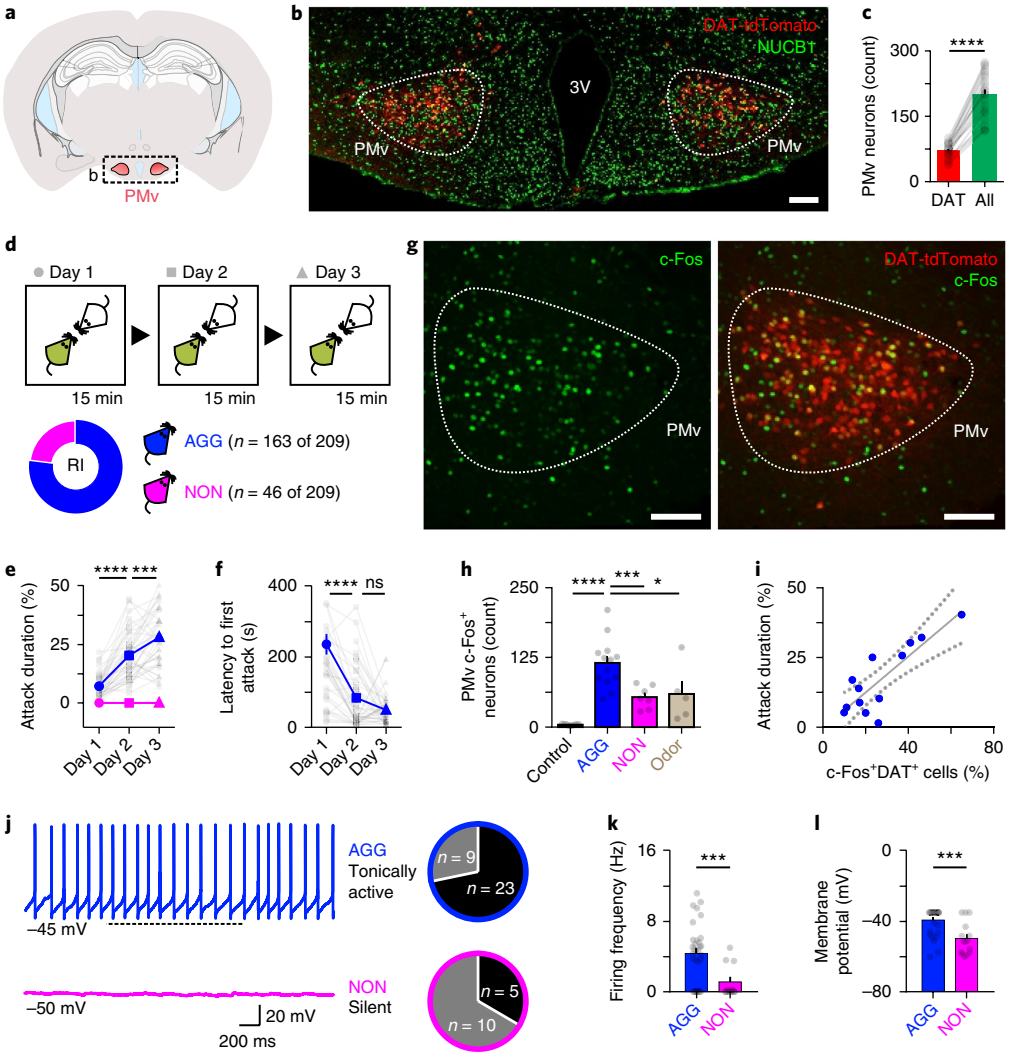

Fig. 1 | Aggression activates PMv^{DAT} neurons, and their electrical activity correlates with aggression phenotype. a, Schematic drawing of PMv at -2.46 mm from bregma in a coronal mouse brain section. **b**, Confocal micrograph of PMv from a DAT-tdTomato mouse section immunostained for the pan-neuronal marker NUCB1. **c**, PMv^{DAT} and total number of PMv neurons ('All') in 14-µm sections ($n = 10$ mice per group, two-tailed unpaired t test, $P < 0.0001$). **d**, Schematic illustration and outcome of aggression screening in RI test. Green, resident; white, intruder. **e**, Attack duration ($n = 42$ AGGs and $n = 17$ NONs, one-way ANOVA with Tukey's test, day 1 vs. day 2, $P < 0.0001$; day 2 vs. day 3, $P = 0.0003$). **f**, Latency to attack ($n = 42$ AGGs, Kruskal–Wallis test followed by Dunn's test for pairwise comparisons, day 1 vs. day 2, $P < 0.0001$; day 2 vs. day 3, $P = 0.8605$). **g**, c-Fos immunoreactivity in AGG in PMv post-RI test against an intruder ($n = 13$ mice; see Supplementary Fig. 1). **h**, Number of c-Fos immunoreactive neurons in PMv with and without introduction of intruder and intruder bedding (control (group of AGGs alone in cage) $n = 9$, AGGs vs. intruder $n = 13$, NONs vs. intruder $n = 7$, AGGs vs. odor (bedding) $n = 5$, one-way ANOVA with Tukey's test, AGGs vs. intruder compared to AGGs alone in cage, $P < 0.0001$; AGGs vs. intruder compared to NONs vs. intruder, $P = 0.0009$; AGGs vs. intruder compared to AGGs exposed to odor in homecage, $P = 0.0120$). **i**, Linear regression of attack duration and proportion of c-Fos$^+$ PMv^{DAT} neurons ($n = 13$, $P = 0.0003$, $R^2 = 0.70$). The dashed grey lines define the 95% confidence intervals. **j**, Representative PMv^{DAT} neuron activity and number of neurons exhibiting tonic firing (black) or a quiescent resting potential (grey) in AGGs and NONs. **k**, Firing frequency ($n = 32$ cells from 11 AGGs, $n = 15$ cells from 7 NONs, two-tailed unpaired t test, $P = 0.0005$). **l**, Membrane potential of PMv^{DAT} neurons in AGGs and NONs ($n = 32$ cells from 11 AGGs, $n = 15$ cells from 7 NONs, two-tailed unpaired t test, $P = 0.0001$). $^*P < 0.05$, $^{**}P < 0.01$, $^{***}P < 0.001$, $^{****}P < 0.0001$; ns, nonsignificant. Data expressed as mean ± s.e.m. Scale bars, 100 µm.

spikes in VMHvl cells, with the majority of these neurons exhibiting PIR (Supplementary Fig. 8j–n). These data identify a combination of intrinsic membrane properties of PMv^{DAT} neurons, their intrinsic recurrent excitatory connectivity, and their reciprocal glutamatergic projections to a major target nucleus (VMHvl), which may act in synergy to contribute to hysteresis in aggression.

PMv target-specific attack and reward behavior. Aggression has been shown to be inherently rewarding in a number of studies[32,33]. Using the real-time place-preference test, we observed a clear bias toward the area associated with ChR2 stimulation of PMv^{DAT} neurons (Supplementary Fig. 9a–c). Conversely, optogenetic eNpHR3-mediated inhibition of PMv^{DAT} neurons resulted in real-time place aversion of even greater amplitude (Supplementary Fig. 9d–f). To elucidate whether modulation of PMv^{DAT} neuron activity can alter other reward- and anxiety-related behaviors, we performed a battery of tests (Supplementary Figs. 10 and 11). Stimulation of PMv^{DAT} cells was found to potentiate cocaine-related conditioned place preference (CPP; Supplementary Fig. 10) suggesting that these cells (or of their downstream targets) may be involved in general

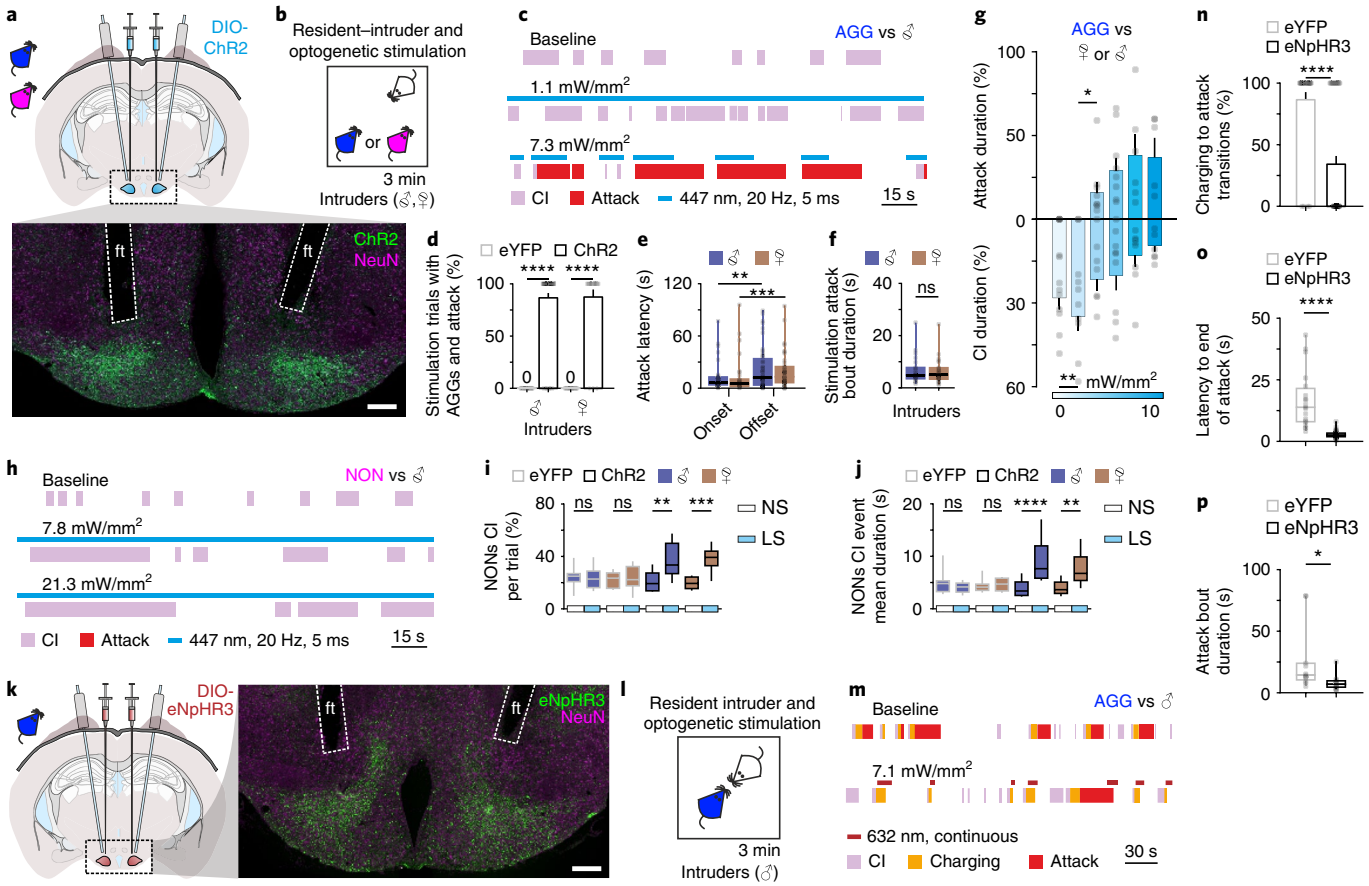

Fig. 2 | PMv^{DAT} neuron activity is necessary and sufficient for aggression. a, Schematic drawing of PMv viral transduction with ChR2 and fiber implants as performed in AGGs and NONs. Confocal micrograph (below) shows ChR2-expressing PMv^{DAT} neurons and immunoreactivity for the neuronal marker NeuN, with optic fiber placement indicated (ft; $n=22$ mice). **b**, Schematic illustration of the behavior protocol used in ChR2-stimulation experiments. Male, ♂; female, ♀. **c**, Sample behavior raster plots of 0 (baseline), low-, and high-intensity ChR2 stimulation in an AGG during RI test. CI, close investiagtion. **d**–**f**, Quantification of aggression parameters. (**d**) Stimulation trials with AGGs and optically evoked attack ($n=24$ trials with 12 eYFP in PMv AGGs and $n=58$ trials with 22 ChR2 in PMv AGGs; eYFP compared to ChR2 AGGs vs. castrated intruders, one-way ANOVA with Tukey's test, $P<0.0001$; $n=24$ trials with 12 eYFP AGGs and $n=22$ trials with 22 ChR2 AGGs; eYFP AGGs compared to ChR2 AGGs vs. ovariectomized intruders, one-way ANOVA with Tukey's test, $P<0.0001$). (**e**) Quantification of attack latency upon photostimulation of 22 ChR2 AGGs (trial average of attack onset against castrated intruders $n=49$, trial average of attack onset against ovariectomized intruders $n=42$, trial average of attack offset against castrated intruders $n=49$, trial average of attack offset against ovariectomized intruders $n=42$; castrated intruder comparison, two-tailed paired t test, $P=0.0049$; ovariectomized intruder comparison, two-tailed paired t test, $P=0.0008$). (**f**) Stimulation attack bout duration (against castrated intruders $n=31$, against ovariectomized intruders $n=22$; two-tailed unpaired t test, $P=0.9806$). **g**, Social behavior as influenced by increasing stimulation power ($n=8$, attack duration, presented comparison; two-tailed paired t test, $P=0.0244$, close investigation (CI) duration, presented comparison; two-tailed paired t test, $P=0.0011$). **h**, Sample behavior raster plots of 0, low-, and high-intensity laser stimulation in a NON during an RI test. **i**,**j**, Quantification of social investigation parameters with (LS) and without (NS) light stimulation. (**i**) CI duration per trial (one-way ANOVA with Tukey's test, comparisons from left to right: $n=12$ per group, $P=0.9471$; $n=8$ per group, $P=0.9809$; $n=10$ per group, $P=0.0034$; $n=10$ per group, $P=0.0009$). (**j**) CI episode duration (one-way ANOVA with Tukey's test, comparisons from left to right: $n=12$ per group, $P=0.9894$; $n=8$ per group, $P=0.9996$; $n=10$ per group, $P<0.0001$; $n=10$ per group, $P=0.0044$). **k**, Schematic drawing of PMv viral transduction with eNpHR3 and fiber implants as performed in AGGs. Confocal micrograph (right) shows eNpHR3^{+} PMv^{DAT} neurons and NeuN immunoreactivity, with optic fiber placement indicated. **l**, Schematic illustration of the behavior protocol used in eNpHR3 stimulation experiments ($n=20$ mice). **m**, Sample behavior raster plots with and without PMv^{DAT} neuron silencing in an AGG during an RI test. **n**–**p**, Quantification of aggression parameters upon eNpHR3-mediated neuron silencing. (**n**) Photoinhibition trials with AGGs and optically terminated attack ($n=30$ trials with 12 eYFP in PMv AGGs and $n=50$ trials with 20 eNpHR3 in PMv AGGs; eYFP compared to eNpHR3 AGGs vs. intact male intruders, two-tailed unpaired t test, $P<0.0001$). (**o**) Latency to end of attack upon photoinhibition ($n=20$ trials with 12 eYFP in PMv AGGs and $n=49$ trials with 20 eNpHR3 in PMv AGGs; eYFP compared to eNpHR3 AGGs vs. intact male intruders, two-tailed unpaired t test, $P<0.0001$). (**p**) Attack bout duration upon photoinhibition in eYFP and eNpHR3 AGGs (average per individual animal, $n=12$ eYFP AGGs and $n=15$ eNpHR3 AGGs, two-tailed unpaired t test, $P=0.0210$). *$P<0.05$, **$P<0.01$, ***$P<0.001$, ****$P<0.0001$; ns, nonsignificant. In bar graphs, data are expressed as mean ± s.e.m. In box-and-whisker plots, center lines indicate medians, box edges represent the interquartile range, and whiskers extend to the minimal and maximal values. Scale bars, 100 µm.

reward-related behaviors. However, anxiety-type behaviors, as tested in the open field arena and the elevated plus maze remained unchanged along PMv^{DAT} neuron activation, inhibition, and genetic lesion (Supplementary Fig. 11).

We next addressed the possibility that separate downstream targets of the PMv mediate these two aspects of aggression: attack behavior and reward. As a first step, we examined the efferent anatomical projections of PMv^{DAT} neurons. Multiple brain nuclei

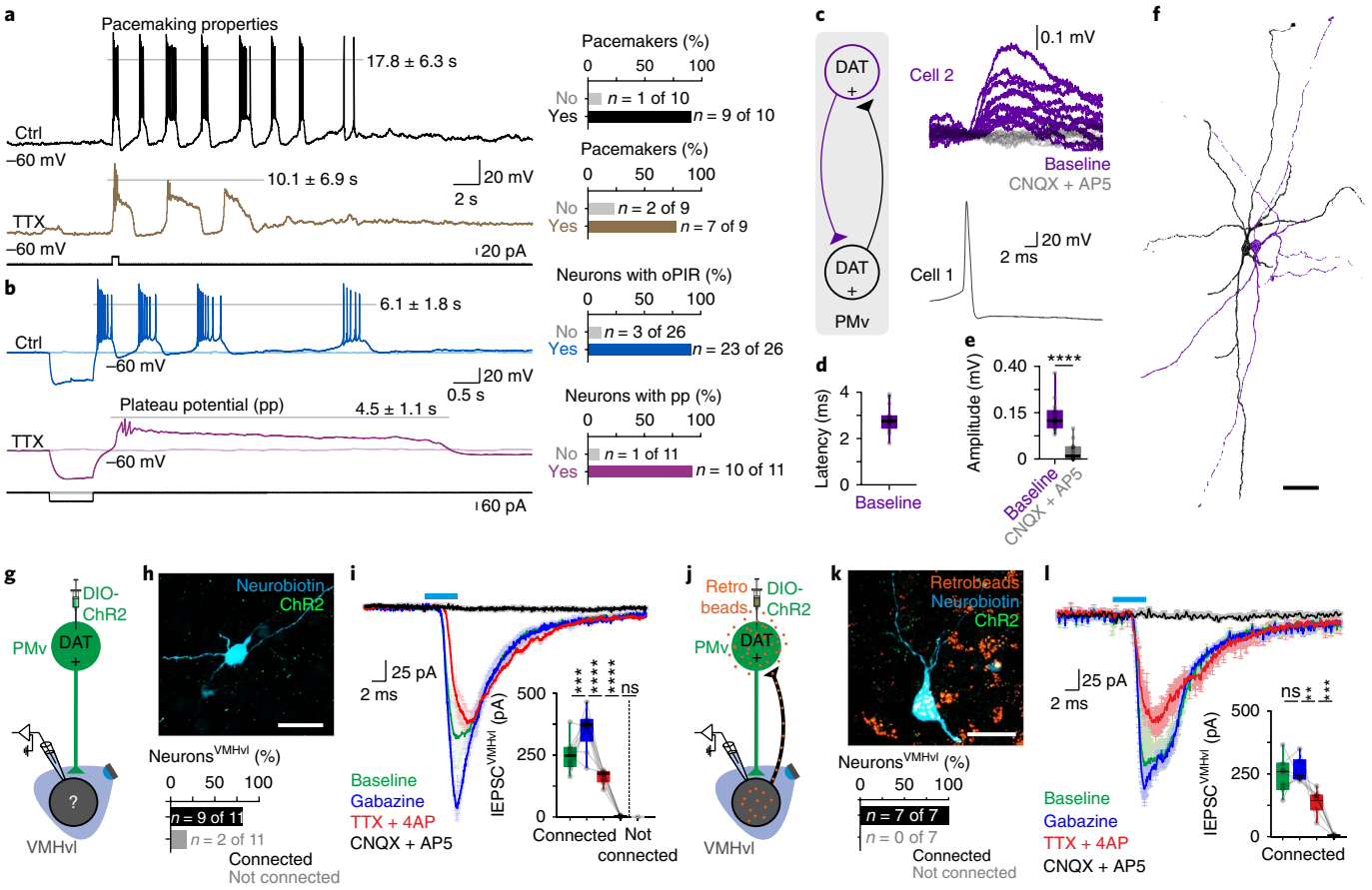

Fig. 3 | Membrane properties and wiring of PMv^{DAT} neurons provide a substrate for persistent activity. a, Brief (0.5-s) positive-current square pulses elicit long-lasting repetitive bursting under control conditions (Ctrl; black) and in the presence of TTX (brown). **b**, Brief (1-s) negative-current square pulses elicit prolonged excitation on baseline (blue) and in the presence of TTX (pink). oPIR, oscillatory postinhibitory rebound; pp, plateau potential. **c**, Paired recordings of neighboring PMv^{DAT} neurons. Evoked action potentials (black) in one neuron induced short-latency excitatory postsynaptic currents (EPSCs) in the other cell (purple), sensitive to glutamate receptor blockers (CNQX and AP5; gray). Reciprocal connections were found in 5 of 11 connected pairs. **d**, Average excitatory postsynaptic potential (EPSP) latency was 2.82 ± 0.14 ms (n = 16 paired recordings). **e**, Average EPSP amplitude was 0.14 ± 0.01 mV (n = 16 paired recordings, two-tailed unpaired t test, $P < 0.0001$). **f**, Cell reconstruction of a synaptically connected pair of PMv^{DAT} neurons exhibiting numerous points of close contacts (n = 3 pairs). **g–i**, Monosynaptic excitatory innervation of VMHvl from PMv^{DAT} neurons. (**g**) Schematic illustration of the experimental design, transducing PMv^{DAT} neurons with ChR2 and evoking postsynaptic light responses in VMHvl in vitro recordings. (**h**) Neurobiotin-stained VMHvl neuron surrounded by ChR2 terminals and responsive to light stimulation (top) and quantification of VMHvl neurons with photostimulation-evoked EPSCs (lEPSCs, bottom). (**i**) Averaged amplitudes of lEPSC evoked on baseline (green), in gabazine (blue), TTX and 4AP (red), in CNQX and AP5 (black), and in nonresponsive neurons (gray; n = 9 connected (c), n = 2 nonconnected (nc); one-way ANOVA with Tukey's test, baseline vs. gabazine, $P = 0.0003$; gabazine vs. TTX + 4AP, $P < 0.0001$; TTX + 4AP vs. CNQX + AP5, $P < 0.0001$). Shaded region represents the standard error. The vertical scale bar defines current and the horizontal scale bar time. **j–l**, Monosynaptic excitatory innervation of VMHvl input neurons to PMv from PMv^{DAT} cells. (**j**) Schematic illustration of the experimental design, transducing PMv^{DAT} neurons with ChR2 with concurrent injection of red retrobeads, and evoking postsynaptic light responses in VMHvl retrobead-containing neurons in in vitro recordings. (**k**) Neurobiotin-stained retrobead-containing VMHvl neuron surrounded by ChR2 terminals and responsive to light stimulation (top) and quantification of similarly selected VMHvl neurons with lEPSCs (bottom). (**l**) Averaged lEPSCs amplitude evoked on baseline (green), in gabazine (blue), TTX and 4AP (red), and in CNQX and AP5 (black; n = 7 per group, one-way ANOVA with Tukey's test: baseline vs. gabazine, $P = 0.9481$; gabazine vs. TTX + 4AP, $P = 0.0012$; TTX + 4AP vs. CNQX + AP5, $P = 0.0001$). Shaded region represents the standard error. The vertical scale bar defines current and the horizontal scale bar time. $^{**}P < 0.01$, $^{***}P < 0.001$, $^{****}P < 0.0001$; ns, nonsignificant. In bar graphs, data are expressed as mean ± s.e.m. In box-and-whisker plots, center lines indicate medians, box edges represent the interquartile range, and whiskers extend to the minimal and maximal values. Scale bars, 50 µm (**f**), 20 µm (**h**,**k**).

receive projections from the PMv[18,20]. Among the innervated areas is the posterior hypothalamus[18]. In mice expressing ChR2-eYFP in PMv^{DAT} neurons, we observed particularly dense innervation of the supramammillary nucleus (SuM; Supplementary Fig. 7a,b,d). The existence of a PMv→SuM projection was further corroborated by injection of green retrobeads into the SuM, which could be observed within ipsilateral PMv^{DAT} neurons (Supplementary Fig. 7l–o). Functional PMv→SuM connectivity was assessed in slice-recording experiments, where the majority of randomly selected SuM neurons (n = 5 of 6) exhibited large-amplitude CNQX- and AP5-sensitive excitatory postsynaptic currents following optogenetic stimulation of PMv^{DAT} neuron terminals (Supplementary Fig. 7e–g).

The SuM has been implicated in reinforcement in self-administration experiments[34,35]. Our results thus indicate that PMv^{DAT} neurons innervate both VMHvl, which is involved in attack behavior[16,36], and SuM, which mediates reward responses. Therefore, we investigated whether anatomically restricted excitation of PMv^{DAT} terminals in

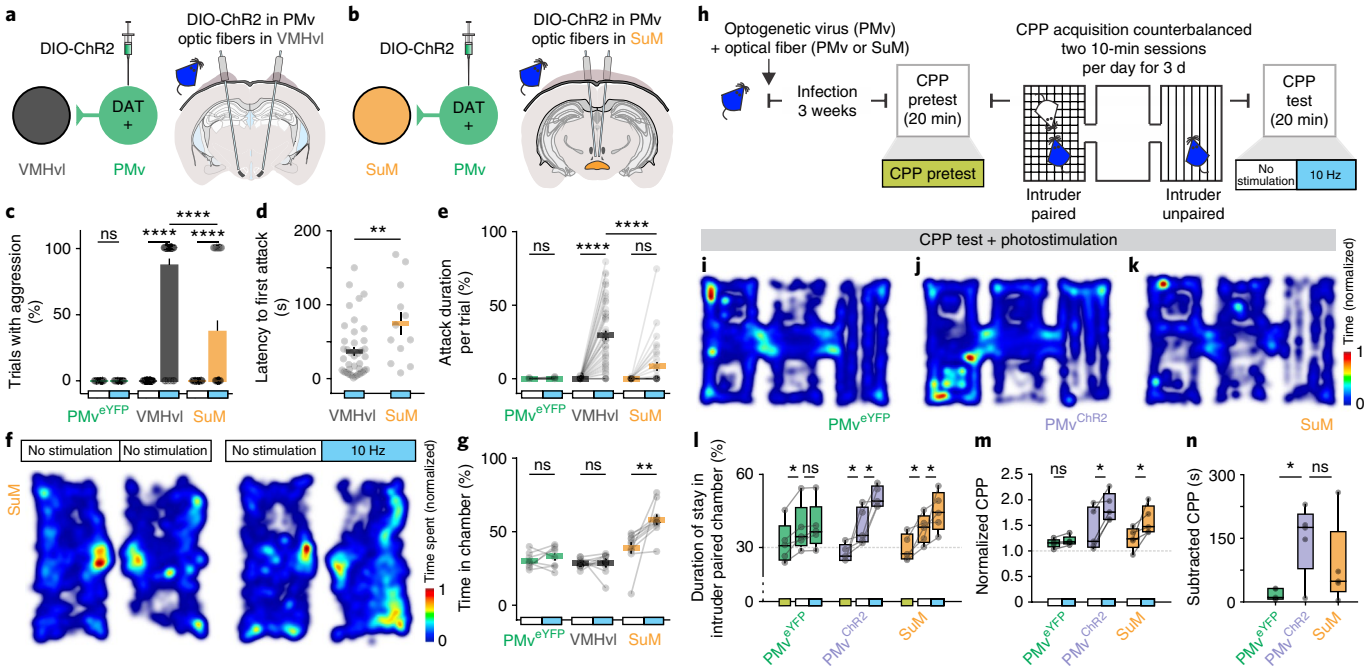

Fig. 4 | Monosynaptic PMv^{DAT} projections in VMHvl and SuM drive aggression intensity and aggression reward. a,**b**, Schematic of the experimental design, transducing PMv^{DAT} neurons with ChR2 and placement of fiberoptic implants in VMHvl (**a**) and SuM (**b**). **c**–**e**, Quantification of aggression parameters. (**c**) Baseline and photostimulation trials with AGGs and optically evoked attack ($n = 20$ trials with 8 eYFP in PMv AGGs with optic fibers in PMv, $n = 48$ trials with 16 ChR2 in PMv AGGs with optic fibers in VMHvl, $n = 30$ trials with 10 ChR2 in PMv AGGs with optic fibers in SuM; baseline vs. photostimulation in the eYFP group, one-way ANOVA with Tukey's test, $P > 0.9999$; baseline vs. photostimulation in the ChR2 in PMv, fibers in VMHvl group, one-way ANOVA with Tukey's test, $P < 0.0001$; baseline vs. photostimulation in the ChR2 in PMv, fibers in SuM group, one-way ANOVA with Tukey's test, $P < 0.0001$; photostimulation in ChR2 in PMv, fibers in VMHvl vs. ChR2 in PMv, fibers in SuM groups, one-way ANOVA with Tukey's test, $P < 0.0001$). (**d**) Latency to first attack upon photostimulation (only trials with attack included, $n = 42$ trials with 16 ChR2 in PMv AGGs with optic fibers in VMHvl, $n = 12$ trials with 10 ChR2 in PMv AGGs with optic fibers in SuM; two-tailed unpaired t test, $P = 0.0071$). (**e**) Quantification of attack duration in baseline and photostimulation trials with AGGs and optically evoked attack ($n = 20$ trials with 8 eYFP in PMv AGGs with optic fibers in PMv, $n = 48$ trials with 16 ChR2 in PMv AGGs with optic fibers in VMHvl, $n = 30$ trials with 10 ChR2 in PMv AGGs with optic fibers in SuM; baseline vs. photostimulation in the eYFP group, one-way ANOVA with Tukey's test, $P > 0.9999$; baseline vs. photostimulation in the ChR2 in PMv, fibers in VMHvl group, one-way ANOVA with Tukey's test, $P < 0.0001$; baseline vs. photostimulation in the ChR2 in PMv, fibers in SuM group, one-way ANOVA with Tukey's test, $P = 0.1373$; photostimulation in ChR2 in PMv, fibers in VMHvl vs. ChR2 in PMv, fibers in SuM groups, one-way ANOVA with Tukey's test, $P < 0.0001$). **f**, Example of real-time place preference in a control (left) and a photostimulation trial (right) with PMv^{DAT} neuron terminal excitation in SuM. **g**, Quantification of time spent in the naturally least-preferred chamber before and after photostimulation ($n = 8$ trials with 8 eYFP in PMv AGGs with optic fibers in PMv, $n = 12$ trials with 12 ChR2 in PMv AGGs with optic fibers in VMHvl, $n = 10$ trials with 10 ChR2 in PMv AGGs with optic fibers in SuM; baseline vs. photostimulation in the eYFP group, one-way ANOVA with Tukey's test, $P = 0.9811$; baseline vs. photostimulation in the ChR2 in PMv, fibers in VMHvl group, one-way ANOVA with Tukey's test, $P > 0.9999$; baseline vs. photostimulation in the ChR2 in PMv, fibers in SuM group, one-way ANOVA with Tukey's test, $P < 0.0001$). **h**, Schematic of the experimental design and aggression-conditioned place-preference procedure, used to test aggression reward. **i**–**k**, Representative CPP heatmaps for PMv^{DAT} neuron stimulation and PMv^{DAT} terminal stimulation in SuM. **l**, Duration of stay in the intruder-paired chamber ($n = 5$ trials with 5 mice per group, one-way ANOVA with Tukey's test; eYFP in PMv AGGs with optic fibers in PMv, pretest vs. CPP test day, no stimulation, $P = 0.0366$; CPP test day, no stimulation vs. CPP test day, stimulation, $P = 0.0869$; ChR2 in PMv AGGs with optic fibers in PMv, pretest vs. CPP test day, no stimulation, $P = 0.0362$; CPP test day, no stimulation vs. CPP test day, stimulation, $P = 0.0354$; ChR2 in PMv AGGs with optic fibers in SuM, pretest vs. CPP test day, no stimulation, $P = 0.0361$; CPP test day, no stimulation vs. CPP test day, stimulation, $P = 0.0359$); color coding as in **h**. **m**, Normalized CPP ($n = 5$ trials with 5 mice per group, two-tailed paired t test comparisons; eYFP in PMv AGGs with optic fibers in PMv CPP test day, no stimulation vs. CPP test day, photostimulation, $P = 0.4088$; ChR2 in PMv AGGs with optic fibers in PMv CPP test day, no stimulation vs. CPP test day, photostimulation, $P = 0.0134$; ChR2 in PMv AGGs with optic fibers in SuM CPP test day, no stimulation vs. CPP test day, photostimulation, $P = 0.0478$). **n**, Subtracted CPP ($n = 5$ trials with 5 mice per group, one-way ANOVA with Tukey's test; eYFP in PMv vs. ChR2 in PMv and fibers in PMv AGGs, $P = 0.0422$; ChR2 in PMv and fibers in PMv AGGs vs. ChR2 in PMv and fibers in SuM AGGs, $P = 0.6229$). $^*P < 0.05$, $^{**}P < 0.01$, $^{***}P < 0.001$, $^{****}P < 0.0001$; ns, nonsignificant. In bar graphs, data are expressed as mean ± s.e.m. In box-and-whisker plots, center lines indicate medians, box edges represent the interquartile range, and whiskers extend to the minimal and maximal values.

either VMHvl or SuM is selectively linked to the attack and reward components of intermale aggressive behavior.

Optogenetic fiber implants were placed above the VMHvl or SuM in DAT-Cre ChR2 PMv-transduced AGGs, to selectively excite either of the two structures in vivo (Fig. 4a,b). Photostimulation of PMv^{DAT} glutamatergic terminals in VMHvl or SuM had a local effect, as quantified through c-Fos expression (Supplementary Fig. 12a–f). Optogenetic stimulation of PMv^{DAT} terminals in the VMHvl during RI tests resulted in similar levels of aggression to that elicited by PMv^{DAT} cell-soma stimulation, measured as the total number of trials with attack behavior and total duration of attack behavior against castrated intruders ($n = 12$–31 mice per group, two-tailed unpaired t test, $P > 0.05$; data not shown). In contrast, stimulation of the PMv^{DAT} terminals in SuM resulted in minimal levels of

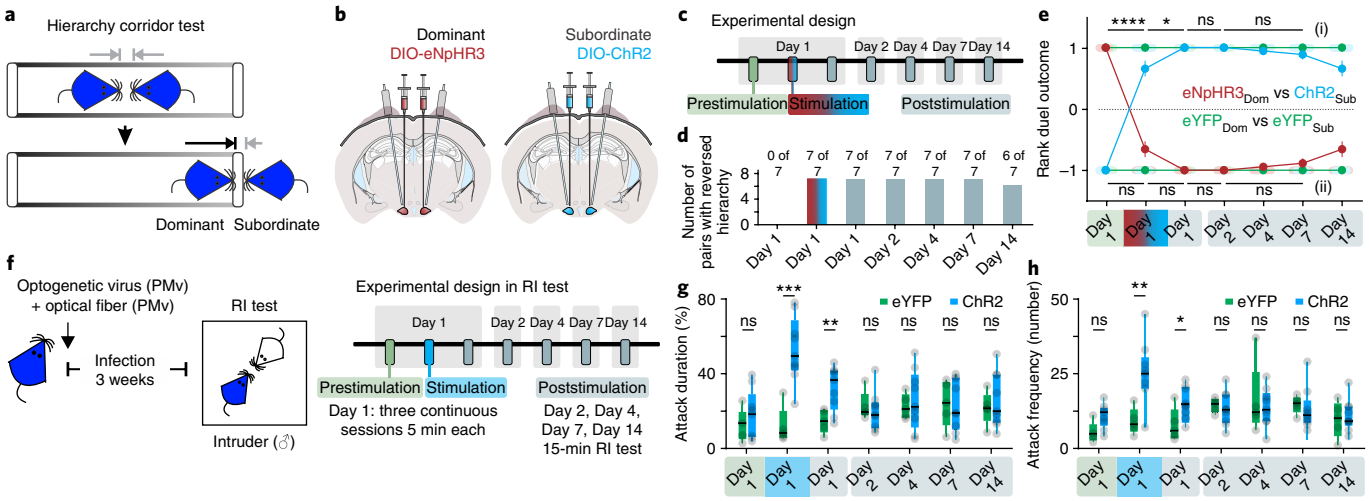

Fig. 5 | Brief manipulation of PMv^{DAT} neuron activity causes a long-lasting switch of intermale hierarchy. a, Schematic of the behavioral test (HCT) used to test intermale hierarchy between male pairs. **b**, Schematic drawing of PMv^{DAT} neuron viral transduction with eNpHR3 and ChR2 in the dominant and subordinate mouse, respectively. **c**, Experimental design indicating behavioral sampling before, during, and after photostimulation in the HCT on different days. **d**, Quantification of male pairs in which hierarchy reversed in the HCT. **e**, Quantification of duel outcomes during the HCT (total of $n=35$ trials per experimental day with 7 ChR2 and 7 eNpHR3 mice, and a total of $n=25$ trials with 5 eYFP mice per experimental day; statistics in the (i) rhodopsin-expressing animals: day 1 prestimulation vs. day 1 during stimulation, $P<0.0001$; day 1 during stimulation vs. day 1 poststimulation, $P=0.0356$; day 1 poststimulation vs. day 2 poststimulation, $P<0.9999$; day 2 poststimulation vs. day 7 poststimulation, $P=0.9464$; one-way ANOVA with Tukey's test and (ii) eYFP-reporter-expressing animals: in all comparisons, $P>0.9999$; one-way ANOVA with Dunn's test to correct for multiple comparisons). Data are expressed as mean ± s.e.m. **f**, Schematic illustration of the behavioral test (RI) used to examine whether a brief manipulation of PMv^{DAT} cells leads to a lasting increase in aggression. Protocol similar to that used in HCT (**c**). **g**,**h**, Quantification of aggression parameters. (**g**) Attack duration (%) upon application of the experimental design used in the HCT test ($n=5$ trials per mice for the eYFP and $n=9$ trials per mice for the ChR2 group; two-tailed unpaired t test, day 1 prestimulation of eYFP vs. day 1 prestimulation of ChR2 animals, $P=0.3327$; day 1 stimulation of eYFP vs. day 1 stimulation of ChR2 animals, $P=0.0005$; day 1 poststimulation of eYFP vs. day 1 poststimulation of ChR2 animals, $P=0.0092$; day 2 poststimulation of eYFP vs. day 2 poststimulation of ChR2 animals, $P=0.6167$; day 4 poststimulation of eYFP vs. day 4 poststimulation of ChR2 animals, $P=0.6529$; day 7 poststimulation of eYFP vs. day 7 poststimulation of ChR2 animals, $P=0.6167$; day 14 poststimulation of eYFP vs. day 14 poststimulation of ChR2 animals, $P=0.9312$). (**h**) Attack frequency (number) on application of the experimental design used in the HCT test ($n=5$ trials per mice for the eYFP and $n=9$ trials per mice for the ChR2 group, two-tailed unpaired t test; day 1 prestimulation of eYFP vs. day 1 prestimulation of ChR2 animals, $P=0.1697$; day 1 stimulation of eYFP vs. day 1 stimulation of ChR2 animals, $P=0.0067$; day 1 poststimulation of eYFP vs. day 1 poststimulation of ChR2 animals $P=0.0387$, day 2 poststimulation of eYFP vs. day 2 poststimulation of ChR2 animals $P=0.6691$, day 4 poststimulation of eYFP vs. day 4 poststimulation of ChR2 animals $P=0.6396$, day 7 poststimulation of eYFP vs. day 7 poststimulation of ChR2 animals $P=0.6409$, day 14 poststimulation of eYFP vs. day 14 poststimulation of ChR2 animals $P=0.6607$). $^*P<0.05$, $^{**}P<0.01$, $^{***}P<0.001$, $^{****}P<0.0001$; ns, nonsignificant. In box-and-whisker plots, center lines indicate medians, box edges represent the interquartile range, and whiskers extend to the minimal and maximal values.

aggression compared to stimulation of PMv^{DAT} terminals in VMHvl or PMv^{DAT} cell somata (Fig. 4c–e). However, PMv^{DAT} terminal stimulation in SuM, but not VMHvl, evoked real-time place preference (Fig. 4f,g; effect not different from PMv^{DAT} cell soma stimulation, $n=8$–15 mice per group, two-tailed unpaired t test, $P>0.05$).

To further investigate the role of PMv^{DAT} neurons and the PMv^{DAT}→SuM projection in aggression reward, an aggression-based CPP procedure[10] was used (Fig. 4h). AGGs were enrolled in a consecutive 5-d CPP test, during which they developed a CPP for the intruder-paired context. The CPP test consisted of a no-stimulation session and a photostimulation session, which were compared to specifically evaluate the role of the circuit in aggression reward. Stimulation of PMv^{DAT} neurons and the PMv^{DAT}→SuM projection promoted the expression of CPP (Fig. 4i–n). Taken together, these experiments show that the PMv monosynaptic targets, VMHvl and SuM, specifically recruit two different behavioral aspects of aggression, the consummatory behavior component (attack) and aggression reward, respectively.

PMv^{DAT} activity and intermale hierarchy. In a final set of experiments, we addressed an issue that has received little attention: whether and how the brain networks involved in intermale aggressive behavior also contribute to its ethological function, establishing social rank among individuals of a population[37–41]. To this end, we tested whether simultaneous manipulation of PMv^{DAT} neuron activity in two individuals with a dominant–subordinate (D-S) relationship can alter the hierarchy within the pair during an agonistic encounter. An adaptation of the tube test[41–43], the hierarchy corridor test (HCT), was used to assess social rank between pairs of AGGs (Supplementary Fig. 13a–d and see Methods). D-S pairs expressing eNpHR3 and ChR2 in PMv^{DAT} neurons, respectively (Fig. 5a,b), were used in a 14-d experimental protocol in the HCT (Fig. 5c). Day 1 included a pretest session in which the D-S relationship was verified, followed by a photostimulation session with concurrent eNpHR3-mediated silencing and ChR2-mediated activation of PMv^{DAT} neurons in the D and S subjects, respectively. The photostimulation session was followed by a period with no photostimulation to assess the persistence of an induced change in the HCT-determined hierarchy score. Lastly, each D-S pair was followed for a period of 2 weeks that included 4 additional HCT sampling days to assess the persistence or reestablishment of hierarchy in the HCT compared with initial conditions. Acute manipulation of PMv^{DAT} neuron activity via photostimulation inverted social rank during the session as measured in the HCT in all pairs. Notably, this shift persisted throughout the entire 14-d period; only 1 of 7 pairs reverted to the original hierarchy

relationship on the last day of testing (Fig. 5d,e, Supplementary Fig. 14a–f, and Supplementary Videos 4–6).

To address whether the switch in hierarchy in the pairs was due to a long-lasting increase in aggression via the ChR2 stimulation of PMv^{DAT} cells, the experimental schedule used in the HCT was applied in RI testing (Fig. 5f). The resident was exposed to a new intruder on each experimental day to ensure high levels of aggression. As expected, optogenetic stimulation of PMv^{DAT} neurons induced an immediate increase in aggression levels. This increase was, however, abolished on the following day, and aggression remained at prestimulation levels for the entire testing period (Fig. 5g–h). Thus, the switch in dominance is unlikely to be the result of a persistent elevation of aggression, and rather is contextually dependent on place and/or the specific pair of mice. These data causally implicate PMv^{DAT} neurons in functional intermale aggression and identify the PMv as an organizing node in the neural circuit underlying behaviors that determine intermale social rank.

Discussion

Identifying the neural circuit organization that drives different behaviors is a central goal in neuroscience, and the advance of in vivo methods and population-targeted manipulation of neurons has dramatically propelled this development. In recent years, several key nuclei involved in aggression have been identified. It remains unknown, however, how the intermale aggression circuit is organized to structure a coherent, stereotyped behavior with a clear ethological function. Previous work has implicated activation of PMv in intermale encounters, yet its role in aggression has remained unidentified[16,18]. Here we show that PMv^{DAT} neurons are a central component of this circuit, with the animal's behavioral responsiveness to PMv^{DAT} manipulation depending on its aggression phenotype (AGG versus NON). Our experiments established a link between PMv^{DAT} neuronal activity and aggression levels. In vitro electrophysiology experiments identify a synergy of regenerative membrane properties and network-driven excitation from both within and outside of the PMv as a compelling candidate for a neural mechanism of hysteresis in aggression, with PMv^{DAT} neurons equipped to amplify brief excitatory input into long bouts of activity. Further work is necessary to determine the extent to which such amplifying mechanisms operate in the intact brain and how they relate to the expression of aggression in animals. Individually, each methodology for manipulating or ablating neurons has limitations that merit consideration[44]. Yet the current data were acquired using several complementary techniques on PMv^{DAT} cells and collectively suggest an important role for this neuronal population in aggression.

In vivo activation, inactivation, and lesion studies demonstrate a causal role for PMv^{DAT} neurons in both the attack and reward features of aggression. We functionally identified that activation of the PMv^{DAT} neuron projection to VMHvl specifically elicits attack, whereas activation of the PMv^{DAT} projection to SuM specifically induces reward rather than aggressive behavior. While the reward component mediated via the PMv^{DAT} cell activation is not specific to aggression, as activation of PMv^{DAT} neurons also modulated cocaine CPP, the current work pinpoints two components of aggressive behavior with overlapping temporal expression whose shared neural point of origin was previously unidentified[45,46].

Lastly, we demonstrated that PMv^{DAT} neurons are directly relevant for the ethological purpose of intermale aggressive behavior, i.e., the establishment of dominion and dominance[47–49]. We showed that a social relationship—the hierarchical status between two males—can be acutely manipulated by interfering with PMv^{DAT} activity with long-lasting consequences. While these experiments offer insight into how plasticity of social relationships can be achieved by strengthening or weakening specific neural circuits, they are constrained by the limitations that laboratory housing imposes on mouse intermale social structure, which is different from that found in populations in the wild[47,48].

Aggression defines social structures throughout the animal kingdom, including those of humans. The present study identifies the PMv^{DAT} neuronal population as a critical component of the circuit that organizes and shapes this fundamental behavior. Whether the role of PMv^{DAT} neurons also extends to other forms of aggression, such as predatory or maternal aggression[1], remains to be investigated. Our own and previous[18] findings of PMv^{DAT} neuron activation in the intruder in the RI test suggest the possibility of PMv^{DAT} neuron involvement in defensive aggression. Future studies will need to determine the potential for adaptive changes in the neural circuit underlying aggression and hierarchy under specific physiological demands and hormonal and neuromodulatory influences, and, critically, further investigate the context in which such manipulations can have an impact on social rank.

Methods

Methods, including statements of data availability and any associated accession codes and references, are available at https://doi.org/10.1038/s41593-018-0153-x.

Received: 14 August 2017; Accepted: 5 April 2018;
Published online: 25 May 2018

References

1. Moyer, K. E. Kinds of aggression and their physiological basis. *Commun. Behav. Biol.* **2**, 65–87 (1968).
2. Yang, T. & Shah, N. M. Molecular and neural control of sexually dimorphic social behaviors. *Curr. Opin. Neurobiol.* **38**, 89–95 (2016).
3. Fernandez-Espejo, E. & Mir, D. Ethological analysis of the male rat's socioagonistic behavior in a resident-intruder paradigm. *Aggress. Behav.* **16**, 41–55 (1990).
4. Natarajan, D., de Vries, H., Saaltink, D. J., de Boer, S. F. & Koolhaas, J. M. Delineation of violence from functional aggression in mice: an ethological approach. *Behav. Genet.* **39**, 73–90 (2009).
5. Hess, W. R. & Brügger, M. Das subkortikale Zentrum der affektiven Abwehrreaktion. (The subcortical center for affective defense reactions.). *Helv. Physiol. Pharmacol. Acta* **1**, 33–52 (1943).
6. Kruk, M. R. et al. Discriminant analysis of the localization of aggression-inducing electrode placements in the hypothalamus of male rats. *Brain Res.* **260**, 61–79 (1983).
7. Lammers, J. H., Kruk, M. R., Meelis, W. & van der Poel, A. M. Hypothalamic substrates for brain stimulation-induced attack, teeth-chattering and social grooming in the rat. *Brain Res.* **449**, 311–327 (1988).
8. Olivier, B. & Wiepkema, P. R. Behaviour changes in mice following electrolytic lesions in the median hypothalamus. *Brain Res.* **65**, 521–524 (1974).
9. Levinson, D. M., Reeves, D. L. & Buchanan, D. R. Reductions in aggression and dominance status in guinea pigs following bilateral lesions in the basolateral amygdala or lateral septum. *Physiol. Behav.* **25**, 963–971 (1980).
10. Golden, S. A. et al. Basal forebrain projections to the lateral habenula modulate aggression reward. *Nature* **534**, 688–692 (2016).
11. Unger, E. K. et al. Medial amygdalar aromatase neurons regulate aggression in both sexes. *Cell Rep.* **10**, 453–462 (2015).
12. Ulrich, R. E. & Craine, W. H. Behavior: persistence of shock-induced aggression. *Science* **143**, 971–973 (1964).
13. Lee, H. et al. Scalable control of mounting and attack by Esr1^{+} neurons in the ventromedial hypothalamus. *Nature* **509**, 627–632 (2014).
14. Donato, J. Jr. et al. Leptin's effect on puberty in mice is relayed by the ventral premammillary nucleus and does not require signaling in Kiss1 neurons. *J. Clin. Invest.* **121**, 355–368 (2011).
15. Motta, S. C. et al. Ventral premammillary nucleus as a critical sensory relay to the maternal aggression network. *Proc. Natl. Acad. Sci. USA* **110**, 14438–14443 (2013).
16. Lin, D. et al. Functional identification of an aggression locus in the mouse hypothalamus. *Nature* **470**, 221–226 (2011).
17. Kollack-Walker, S. & Newman, S. W. Mating and agonistic behavior produce different patterns of Fos immunolabeling in the male Syrian hamster brain. *Neuroscience* **66**, 721–736 (1995).
18. Soden, M. E. et al. Genetic isolation of hypothalamic neurons that regulate context-specific male social behavior. *Cell Rep.* **16**, 304–313 (2016).
19. Van den Berg, M. J., Ter Horst, G. J. & Koolhaas, J. M. The Nucleus premammillaris ventralis (Pmv) and aggressive-behavior in the rat. *Aggress. Behav.* **9**, 41–47 (1983).

20. Canteras, N. S., Simerly, R. B. & Swanson, L. W. Projections of the ventral premammillary nucleus. *J. Comp. Neurol.* **324**, 195–212 (1992).
21. Cavalcante, J. C., Bittencourt, J. C. & Elias, C. F. Distribution of the neuronal inputs to the ventral premammillary nucleus of male and female rats. *Brain Res.* **1582**, 77–90 (2014).
22. Ziegler, D. R., Cullinan, W. E. & Herman, J. P. Distribution of vesicular glutamate transporter mRNA in rat hypothalamus. *J. Comp. Neurol.* **448**, 217–229 (2002).
23. Meister, B. & Elde, R. Dopamine transporter mRNA in neurons of the rat hypothalamus. *Neuroendocrinology* **58**, 388–395 (1993).
24. Blanchard, D. C. & Blanchard, R. J. Ethoexperimental approaches to the biology of emotion. *Annu. Rev. Psychol.* **39**, 43–68 (1988).
25. Curran, T. & Morgan, J. I. Fos: an immediate-early transcription factor in neurons. *J. Neurobiol.* 26, 403–412 (1995).
26. Polston, E. K. & Erskine, M. S. Patterns of induction of the immediate-early genes *c-fos* and *egr-1* in the female rat brain following differential amounts of mating stimulation. *Neuroendocrinology* **62**, 370–384 (1995).
27. Barbosa, F. et al. Hysteresis effect in the processing of facial expressions of emotion and its neurophysiological correlates. *Psychophysiology* **50**, S132 (2013).
28. McCormick, D. A. & Pape, H. C. Properties of a hyperpolarization-activated cation current and its role in rhythmic oscillation in thalamic relay neurones. *J. Physiol. (Lond.)* **431**, 291–318 (1990).
29. Falkner, A. L., Dollar, P., Perona, P., Anderson, D. J. & Lin, D. Decoding ventromedial hypothalamic neural activity during male mouse aggression. *J. Neurosci.* **34**, 5971–5984 (2014).
30. Yang, T. et al. Social control of hypothalamus-mediated male aggression. *Neuron* **95**, 955–970.e4 (2017).
31. Tong, Q. et al. Synaptic glutamate release by ventromedial hypothalamic neurons is part of the neurocircuitry that prevents hypoglycemia. *Cell Metab.* **5**, 383–393 (2007).
32. Fish, E. W., DeBold, J. F. & Miczek, K. A. Escalated aggression as a reward: corticosterone and GABA(A) receptor positive modulators in mice. *Psychopharmacology (Berl.)* **182**, 116–127 (2005).
33. Burgdorf, J. et al. Ultrasonic vocalizations of rats (*Rattus norvegicus*) during mating, play, and aggression: behavioral concomitants, relationship to reward, and self-administration of playback. *J. Comp. Psychol.* **122**, 357–367 (2008).
34. Ikemoto, S., Witkin, B. M., Zangen, A. & Wise, R. A. Rewarding effects of AMPA administration into the supramammillary or posterior hypothalamic nuclei but not the ventral tegmental area. *J. Neurosci.* **24**, 5758–5765 (2004).
35. Ikemoto, S. & Bonci, A. Neurocircuitry of drug reward. *Neuropharmacology* **76** Pt B, 329–341 (2014).
36. Spiteri, T. et al. The role of the estrogen receptor alpha in the medial amygdala and ventromedial nucleus of the hypothalamus in social recognition, anxiety and aggression. *Behav. Brain Res.* **210**, 211–220 (2010).
37. Desjardins, C., Maruniak, J. A. & Bronson, F. H. Social rank in house mice: differentiation revealed by ultraviolet visualization of urinary marking patterns. *Science* **182**, 939–941 (1973).
38. Wong, M. & Balshine, S. Fight for your breeding right: hierarchy re-establishment predicts aggression in a social queue. *Biol. Lett.* **7**, 190–193 (2011).
39. Bernstein, I. S., Rose, R. M., Gordon, T. P. & Grady, C. L. Agonistic rank, aggression, social-context, and testosterone in male pigtail monkeys. *Aggress. Behav.* **5**, 329–339 (1979).
40. Young, C., Majolo, B., Schulke, O. & Ostner, J. Male social bonds and rank predict supporter selection in cooperative aggression in wild Barbary macaques. *Anim. Behav.* **95**, 23–32 (2014).
41. van den Berg, W. E., Lamballais, S. & Kushner, S. A. Sex-specific mechanism of social hierarchy in mice. *Neuropsychopharmacology* **40**, 1364–1372 (2015).
42. Lindzey, G., Winston, H. & Manosevitz, M. Social dominance in inbred mouse strains. *Nature* **191**, 474–476 (1961).
43. Zhou, T. et al. History of winning remodels thalamo-PFC circuit to reinforce social dominance. *Science* **357**, 162–168 (2017).
44. Südhof, T. C. Reproducibility: Experimental mismatch in neural circuits. *Nature* **528**, 338–339 (2015).
45. Hoebel, B. G. The neural and chemical basis of reward - new discoveries and theories in brain control of feeding, mating, aggression, self-stimulation and self-injection. *J. Soc. Biol. Struct.* **5**, 397–408 (1982).
46. Gil, M., Nguyen, N. T., McDonald, M. & Albers, H. E. Social reward: interactions with social status, social communication, aggression, and associated neural activation in the ventral tegmental area. *Eur. J. Neurosci.* **38**, 2308–2318 (2013).
47. Anderson, P. K. Density, social structure, and nonsocial environment in house-mouse populations and the implications for regulation of numbers. Trans. *N. Y. Acad. Sci.* **23**, 447–451 (1961).
48. Singleton, G. R. The social and genetic-structure of a natural colony of house mice, *Mus musculus*, at Healesville Wildlife Sanctuary. *Aust. J. Zool.* **31**, 155–166 (1983).
49. Chambers, L. K., Singleton, G. R. & Krebs, C. J. Movements and social organization of wild house mice (*Mus domesticus*) in the wheatlands of northwestern Victoria, Australia. *J. Mamm.* **81**, 59–69 (2000).

Acknowledgements

The authors thank I. Lazaridis for advice on optogenetics; C. Bellardita and V. Caggiano for advice on hardware, software coding, and experiments; and K. Ampatzis for advice on illustrations. We thank members of the Broberger laboratory for discussion during the preparation of this manuscript; N.G. Larsson and O. Kiehn for sharing the DAT-Cre and *loxP*-flanked tdTomato mice, respectively; and K. Fuxe for sharing reagents. We thank M. Wendel (Dept. of Dental Medicine, Karolinska Institutet) for generously sharing primary NUCB-1 antiserum. The authors acknowledge I. Lazaridis, C. Bellardita, and A. El Manira for providing insightful suggestions on the manuscript. This study was supported by a European Research Council starting grant (261286), the Swedish Research Council (2014-3906), the Strategic Research Program in Diabetes at Karolinska Institutet, *Hjärnfonden* (the Swedish Brain Foundation), Novo Nordisk Fonden, and internal funds from Karolinska Institutet.

Author contributions

S.S., G.S., and P.W. designed, performed, and analyzed experiments. J.P. performed neuron reconstructions. G.F. and C.B. designed experiments. S.S. and C.B. wrote the manuscript. All authors reviewed the manuscript.

Competing interests

The authors declare no competing interests.

Additional information

Supplementary information is available for this paper at https://doi.org/10.1038/s41593-018-0153-x.

Reprints and permissions information is available at www.nature.com/reprints.

Correspondence and requests for materials should be addressed to S.S. or C.B.

Publisher's note: Springer Nature remains neutral with regard to jurisdictional claims in published maps and institutional affiliations.

Methods

Animals. All animal experiments had received approval from the local ethical board, *Stockholms Norra Djurförsöksetiska Nämnd*, and were performed in accordance with the European Communities Council Directive of November 24, 1986 (86/609/EEC). Wild-type mice with C57BL/6J and BALB/c background were used, in addition to previously generated C57BL/6J *Slc6a*^{Cre} (DAT-Cre) knockin[50] and *loxP*-flanked tdTomato mice (The Jackson Laboratory, strain datasheet 007909). Animals were grouped-housed, up to five per cage, in a temperature-controlled (23 °C) and humidity-controlled (55%) environment, on a 12 h light, 12 h dark cycle with ad libitum access to food and water. Cages were changed on a weekly basis.

In situ hybridization. DAT-Cre-*loxP*-flanked-tdTomato mice were killed by decapitation, and the brains were rapidly removed and frozen on dry ice. We cut 10-µm-thick coronal sections using a cryostat and thaw-mounted them onto SuperFrost glass slides. Sections were fixed in 4% PFA for 15 min at 4 °C and then dehydrated through incubation in 50% EtOH (1 × 5 min), 70% EtOH (1 × 5 min) and lastly 100% EtOH (2 × 5 min). Slides were air-dried for 10 min and a hydrophobic barrier was created around each section using the ImmEdge pen (Vector Laboratories). In situ hybridization was performed using a modification of the RNAScope (Advanced Cell Diagnostics) protocol. Pretreat 4 (ACDBio, RNAscope Fluorescent Multiplex Reagent Kit, 320850) was added to entirely cover the sections for 30 min at room temperature (23 °C). After PBS washing, sections were incubated with Mm-Slc6a3-C2 (ACDBio, 315441-C2) and tdTomato (ACDBio, 317041) RNAscope probes for 2 h at 40 °C using the HybEZ Humidifying System. The following incubation steps were then performed: Amp 1-FL for 30 min at 40 °C, Amp 2-FL for 15 min at 40 °C, Amp 3-FL for 30 min at 40 °C, and Amp 4-FL-AltB for 15 min at 40 °C (320850). Wash buffer (ACDBio, 320850) was used to rinse the slides after each step. Sections were incubated with DAPI solution (320850) for 30 s at room temperature and ProLong Gold Antifade Mountant (ThermoFisher Scientific) was added before placing the coverslips. Quantification of mRNA coexistence within cells was performed on confocal *z*-stack PMv images acquired at 40 × magnification.

Viral vectors. For channelrhodopsin optogenetic studies, animals were injected in the PMv with 400 nL of AAV5-EF1a-DIO-hChR2(H134R)-eYFP-WPRE-hGH (Addgene 20298), 8.41×10^{12} genomic copies per mL. For halorhodopsin-mediated neuronal silencing, animals were injected with 400 nL of AAV5-EF1a-DIO-eNpHR3.0-eYFP-WPRE-hGH (Addgene 26966), 7.02×10^{12} genomic copies per mL. The control groups in optogenetic were injected with 400 nL of AAV5-EF1a-DIO-eYFP-WPRE-hGH (Addgene 27056), 5.82×10^{12} genomic copies per mL. The ChR2, eNpHR3, and eYFP AAV5 were prepared by the University of Pennsylvania Vector Core. For targeted cell ablation of DAT^{+} PMv neurons, animals were injected in PMv with 300 nL of AAV5-EF1a-DIO-mCherry-dtA, 3.46×10^{12} genomic copies per mL, and the AAV5-dta was prepared by the viral vector core at the University of North Carolina. Viral injections were performed bilaterally unless stated otherwise. Control injections of the Cre dependent viral constructs were performed in C57 wild-type mice; no fluorophore expression was detected in these animals ($n = 12$).

Stereotactic surgery and viral gene transfer. Adult DAT-Cre mice of 3 to 6 months age (sexually inexperienced) were stereotactically injected with a virus and, when purposed implanted with fiber implants for in vivo optogenetic behavior experiments, and were individually housed for 2 weeks postsurgery. Animals were anesthetized with isoflurane (1–5%) and placed in a stereotaxic frame (David Kopf Instruments). Virus was injected into the PMv bilaterally using a pulled-glass capillary (World Precision Instruments) by nanoliter pressure injection at a flow rate of 50 nL per min (Micro4 controller, World Precision Instruments; Nanojector II, Drummond Scientific). Stereotactic injection coordinates to target the PMv were obtained from the Paxinos and Franklin atlas (bregma, −2.45 mm; midline, ±0.6 mm; dorsal surface, −5.5 mm). Ferrules and fiber-optic patch cords were purchased from Thorlabs and Doric Lenses respectively. The virus-injected animals were housed individually in a reversed light/dark room during a 2- to 4-week recovery period, and then examined behaviorally and histologically.

Optogenetics. In optogenetic experiments, subjects were coupled via a ferrule patch cord to a ferrule on the head of the mouse using a zirconia split sleeve (Doric Lenses). The optical fiber was connected to a laser (447 nm for ChR2; 635 nm for eNpHR3; CNI-MLL-III-447-200-5-LED and CNI-MLL-III-635-200-5-LED, CNI lasers 200 mW) via a fiber-optic rotary joint (FRJ_1 × 1_FC-FC, Doric Lenses) to avoid twisting of the cable caused by the animal's movement. After a testing session, DAT-Cre animals were uncoupled from the fiber-optic cable and returned to a housing room. The frequency and duration of photostimulation were controlled using custom-written LabView software. Laser power was controlled by dialing an analog knob on the power supply of the laser sources. Light power was measured from the tip of the ferrule in the patch cord before being installed in the brain (the ferrule-connector system) at different laser output settings, using an optical power and energy meter and a photodiode power sensor (Thorlabs). Upon identification of the fiber placement coordinates in brain tissue slides, irradiance (light intensity) was calculated using the brain tissue light transmission calculator (http://www.stanford.edu/group/dlab/cgi-bin/graph/chart.php) using laser power measured at the tip and the distance from the tip to the target brain region measured by histology. Animals showing no detectable viral expression in the target region and/or ectopic fiber placement were excluded from analysis. In some experiments, animals were photostimulated with a train of 473 nm light (20 Hz, 5 ms, 5 min) 45 min before perfusion in the absence of an intruder at an intensity that had evoked a behavioral phenotype in the final testing session. Then, brain sections were immunohistochemically labeled for c-Fos to identify optogenetically activated cells.

Behavioral tests. All behavioral tests were performed during the dark phase and under dim red light between 1 h after initiation of the dark phase and 2 h before initiation of the light phase. Mice were acclimated to the testing facility for 1 h before testing. Behaviors were recorded using a digital video recording unit and scored using EthoVision (Noldus Information Technology).

Open field test (OFT). OFTs were performed in a white acrylic glass box (45 × 45 × 40 cm) with an overhead lamp directed to the center of the field, providing 120 lx of illumination on the floor of the arena. Each mouse was placed in the corner of the apparatus and locomotion parameters were recorded for 20 min. All subjects went through a single 5-min session before the OFT day for acclimatization.

Elevated plus maze (EPM). The EPM test was performed using a polyvinyl chloride maze comprising a central part (5 × 5 cm), two opposing open arms (32.5 × 5 cm each), and two opposing closed arms (32.5 × 5 × 32.5 cm each). The apparatus was set to a height of 50 cm, and the open arms were provided with uniform overhead illumination of 6 lx. Mice were placed in an open arm, close to the center and facing the closed arms, and video recordings were performed for a total duration of 20 min. A day before the test, mice were placed in the arena for a total duration of 5 min for acclimatization.

Resident–intruder (RI) test. RI tests were initiated at 2 to 4 weeks postsurgery and repeated weekly for 2 to 5 weeks. Mouse cages were not cleaned for a minimum of 3 d before the behavioral test. One to three intruders were individually introduced to a DAT-Cre mouse in a testing session in a random order with respect to gender, with a 5 min interval between intruders. The strains of intruders were: intact males, castrated males, ovariectomized females (BALB/c and C57BL/6J), and females in estrus (stage of cycle was defined by inspection of vaginal smears, performed on the day of the experiment). Subjects involved in the RI test were exposed to three experimental days of the test, resulting in multiple measurements per resident per type of intruder.

ChR2-mediated activation in RI. After the introduction of an intruder, a virus-injected animal (AGG or NON) was recorded for 3–10 min to assess baseline behavior toward each intruder. The baseline recording was followed by photostimulation trials (maximum 20 min in duration) with varying irradiance (intensity), stimulation intervals, distance, orientation, and recent behavior history of the two animals at the onset of photostimulation. The AAV5-DIO-eYFP-injected and AAV5-DIO-ChR2-injected experimental animals were processed in random order.

eNpHR3-mediated silencing in RI. DAT-Cre AGG males expressing eNpHR3 or control eYFP were introduced to one to four male intruders in three acclimation sessions without photostimulation to assess baseline aggression as well as to augment aggressiveness. Testing sessions were initiated with recordings in the absence of laser stimulation to assess baseline behavior toward each intruder on the day of the experiment. In photostimulation trials, irradiance (intensity) ranging from 3.4 to 21.7 mW/mm^2 was delivered continuously in varying intervals (typically 2–10 s) depending on the phase of the resident–intruder interaction. To examine whether photostimulation during charging stopped escalation to attack, residents were photostimulated during body realignment to gain access to the back of the intruder.

Real-time place-preference and -aversion. Mice were placed in a custom-made behavioral arena (35 × 35 × 25 cm black acrylic glass) for 15 min. In experiments of ChR2 stimulation, the least-preferred chamber was assigned as the stimulation side. In experiments of eNpHR3 stimulation, the preferred chamber was assigned as the stimulation side. The mouse was placed in the nonstimulated side at the onset of the experiment and constant laser stimulation was delivered each time the mouse crossed into the stimulation side of the chamber until the mouse moved back into the nonstimulation side (20 Hz 5 ms for ChR2, continuous for eNpHR3).

Aggression CPP. The aggression CPP protocol was used as described previously[10,51]. It consisted of three phases. The first phase was a pretest session during which animals freely explored the three-chamber area. AGGs with no individual preference for any of the three chambers were further used. The second phase was a 3-d acquisition phase, during which animals were exposed to the

intruder-paired chamber and the nonpaired chamber twice daily, alternating the sessions in consecutive days. In the last phase, the test day was composed of a morning and an afternoon session, 2 h apart. In the morning session, the developed CPP was assessed in all animals with no stimulation, and the afternoon session was a repetition of the morning session under the exact same conditions but with photostimulation. This allowed for paired comparisons among individuals and an additional control step, validating that the intruder-paired chamber induced CPP in all subjects. Analysis of the time duration in each chamber was used to identify CPP to the intruder-paired chamber. For optogenetic experiments, photostimulation was performed throughout the duration of the test (20 min) at 10 Hz, 5 ms using a laser power output per individual that had been previously shown to evoke attack in RI tests or real-time place-preference in RTPP tests. Additionally, locomotion parameters were assessed to control for exploratory behavior, and were found equal among groups. Behavioral analysis of aggression CPP was performed by comparison of (i) the duration of stay (% and in seconds) in the intruder-paired chamber in the pretest vs. test with no stimulation vs. test with stimulation; (ii) normalized CPP (the test with no stimulation phase duration spent in the intruder-paired chamber divided by the pretest phase duration spent in the intruder-paired chamber, and similarly, the test with stimulation phase duration spent in the intruder-paired chamber divided by the pretest duration spent in the intruder-paired chamber); and lastly, (3) subtracted CPP (test with stimulation phase duration spent in the intruder-paired chamber minus the test with no stimulation phase duration spent in the intruder-paired chamber).

Cocaine CPP. The cocaine CPP protocol consisted of three phases. The first phase (pretest) was performed to assess the lack of predetermined preference to any of the three chambers of the CPP arena. The second phase included the CPP acquisition and consisted of two successive days with four conditioning trials in total. The morning (between 9:00 a.m. and 11:00 a.m.) and afternoon (between 3:00 p.m. and 5:00 p.m.) sessions consisted of mice confined to one chamber for 20 min, paired with an intraperitoneal injection of cocaine (10 mg/kg) or saline; the afternoon session was counterbalanced with saline or cocaine. The third phase was the test day, and included a morning session during which the developed CPP was assessed in all animals with no stimulation, and the afternoon session was a repetition of the morning session under the exact same conditions but with photostimulation. This allowed for paired comparisons among individuals and an additional control step, validating the cocaine-paired chamber induced CPP in all subjects. Analysis of the time duration in each chamber was used to identify CPP to the cocaine-paired chamber. For optogenetic experiments, photostimulation was performed throughout the duration of the test (20 min) at 10 Hz, 5 ms using a laser power output per individual that had been previously shown to evoke attack in RI tests or real-time place-preference in RTPP tests. Lastly, locomotion parameters were assessed to control for exploratory behavior and were found equal among groups. We purchased (-)-cocaine hydrochloride (RTI log no: 12295-1022-38 C) from RTI International, NIDA, NIH, USA.

Hierarchy corridor test (HCT). Behavioral tests were initiated at 3 to 4 weeks postsurgery and were repeated for the defined behavioral sampling days of our protocol. Only AGGs were involved in these experiments. To assess the validity of the test in assessing hierarchy, 12 pairs performed baseline repeated sessions upon which the robustness of the test was characterized (Supplementary Fig. 12a,b). The HCT arena was custom-made, and composed of a long narrow corridor 1 m in length and of variable width. The width was adjusted for every mouse pair entering the HCT challenge, depending on the weight/size of the subjects and was typically 28 mm. The corridor was lit with dim red light by a 1-m-long LED strip placed below the total length of the corridor. At each end of the corridor two antechambers (12 × 20 × 20 cm) were attached with a closed gate. Upon vertical retraction of the gate, the subjects gained access to the corridor, which they traversed until reaching the midpoint where a second gate was present. Upon both subjects reaching the center of the corridor, the midpoint gate was retracted vertically and subjects' social interaction was monitored. The end of a duel was defined as the point when the body of one of the two mice was fully displaced from the corridor while the body of the other mouse was still present in the corridor. A duel typically lasted 40 s, after which mice were replaced to their initial position/room. A short delay (~2 min) was imposed between consecutive sessions. Each session, before, during, and after stimulation, was composed of 5 trials. Pairs in the HCT tests included a heavier-weight, dominant eNpHR3^{+} subject and a lighter, ChR2^{+} subordinate (Supplementary Fig. 12c); net body weight difference was 8 ± 0.81 g. Suitable dominant/subordinate pairs for the HCT were identified from pre-existing groups of ChR2-eYFP- and eNpHR3-eYFP-transduced AGGs. All mice went through a habituation session in the HCT arena before initiation of the HCT, where they freely explored the arena space with all gates open and in the absence of another mouse, gaining experience of space and the three different HCT compartments. Mice used in the HCT had no preference for any of the chambers (Supplementary Fig. 12d).

Brain slice electrophysiology. Acute slices of the mediobasal hypothalamus were prepared from adult DAT-tdTomato mice (own breeding) that had been previously identified by aggression phenotype in the RI test. Slices were cut on a vibratome (Leica VT1000S) to 250-µm thickness and continuously perfused with oxygenated aCSF containing (in mM): 127 NaCl, 2.0 KCl, 1.2 NaH_2PO_4, 26 $NaHCO_3$, 1.3 $MgCl_2$, 2.4 $CaCl_2$, and 10 D-glucose, at room temperature during recording. Each slice was exposed only to a single bath application of pharmacological compounds and was used for a single experiment. Whole-cell current- and voltage-clamp recordings were performed with micropipettes filled with intracellular solution containing (in mM), 140 potassium-gluconate, 10 KCl, 10 HEPES, 10 EGTA, and 2 Na_2ATP (pH 7.3), with KOH. Recordings were performed using a Multiclamp 700B amplifier, a DigiData 1440 digitizer, and pClamp10.2 software (Molecular Devices). Slow and fast capacitive components were automatically compensated for. Access resistance was monitored throughout the experiments, and neurons in which the series resistance exceeded 15 MΩ or changed ≥20% were excluded from the statistics. Liquid junction potential was 16.4 mV and not compensated for. The recorded current was sampled at 20 kHz and filtered at 2 kHz.

For in vitro optogenetics during slice whole-cell recordings, photostimulation was generated through a 3.4-W 447-nm or 632-nm LED mounted on the microscope oculars and delivered through the objective lens. Photostimulation was controlled via the analog outputs of a DigiData 1440 A, enabling control over the duration and intensity. The photostimulation diameter through the objective lens was ~350 µm with illumination intensity typically scaled to 3 mW/mm^2.

Reagents used in slice electrophysiology experiments; Neurobiotin tracer (Vector Laboratories) was used in combination with streptavidin, DyLight 405-conjugated (21831 Thermo Scientific) or Avidin-FITC (43-4411 Invitrogen). TTX was purchased from Alomone Labs. CNQX, AP5, SR 95531 (gabazine), ML-218 hydrochloride, and ZD-7288 were purchased from Tocris, and 4AP was purchased from Sigma. Matlab and OriginPro8 were used for electrophysiological data analysis.

Immunohistochemistry. Mice were anesthetized with sodium pentobarbital (200 mg/kg, i.p., Sanofi-Aventis, France), then transcardially perfused with 10 mL Ca^{2+}-free Tyrode's solution (37 °C) containing 0.2% heparin, followed by 10 mL fixative (4% paraformaldehyde and 0.4% picric acid in 0.16 M phosphate buffer (PBS), 37 °C), then 50 mL ice cold fixative. Whole brains were dissected, immersed in ice-cold fixative for 90 min, and then stored in 0.1 M PBS (pH 7.4) containing 20% sucrose, 0.02% bacitracin, and 0.01% sodium azide for 3 d, before freezing with CO_2. Coronal sections were cut at a thickness of 14 µm using a cryostat (Microm, Walldorf, Germany) and thaw-mounted onto gelatin-coated glass slides. For indirect immunofluorescence staining (performed at room temperature unless otherwise specified), air-dried sections were washed in 0.01 M PBS for 30 min before incubation with anti-nucleobindin-1 primary antisera[52,53], kindly provided by M. Wendel, diluted in PBS containing 0.3% Triton X-100 and 1% BSA for 16 h at 4 °C. The slides were then washed for 30 min in PBS followed by 2 h incubation with Alexa Fluor 488-conjugated donkey anti-rabbit secondary antisera (1:500; Invitrogen). Slides were incubated with the nuclear marker 4',6-diamidino-2-phenylindole (DAPI; Invitrogen) diluted 1: 10,000 in PBS for 5 min before a final wash for 30 min in PBS and mounted with glycerol containing (2.5% DABCO; Sigma, St Louis, MO, USA). This method was used with the following antibodies: NeuN was detected with primary antibody rabbit anti-NeuN (1:500; Cell Signaling, D4G40), eYFP was detected with chicken anti-GFP (1:500; Aves Labs, GFP-1020), ERα was detected with rabbit anti-ERα (1:200; Santa Cruz Biotechnology, sc-542).

For the DAT immunostaining, sections were washed in TBS (0.1 M Tris-HCl, 0.15 M NaCl, pH 7.5), incubated 10 min in 1% H_2O_2-TBS to quench endogenous peroxidases and washed in TBS. Following permeabilization in 1% DMSO–0.3% Triton-TBS for 30 min, section were washed in TNT (0.05% Tween-TBS) and incubated for 2 h in TNB blocking buffer (0.5% blocking reagent-TBS, Perkin Elmer). Sections were then kept at 4 °C in rat anti-DAT antibody (MAB369, Millipore) solution (1:1,000 in TNB). After TNT washing, sections were incubated for 1 h at room temperature in goat anti-rat HRP-conjugated secondary antibody (AP136P, Chemicon) solution (1:500 in TNB). Brain slices were then washed in TNT and covered for 10 min with TSA working solution (Fluorescein Plus Amplification Reagent, 1:100 in Plus Amplification Diluent, Perkin Elmer). Following TNT washing, slides were mounted using 2.5% DABCO-DMSO.

To perform c-Fos immunostaining, mice were deeply anesthetized with sodium pentobarbital (as described above) and perfused transcardially with 4% (weight/vol) ice-cold paraformaldehyde in 0.1 M PBS. Brains were postfixed in the same solution and 40-µm-thick coronal slices were cut on the vibratome (Leica, Germany). Two PMv coronal sections per animal were selected to perform c-Fos immunostaining as follows. Sections were washed in TBS (100 mM Tris-Cl, 150 mM NaCl, pH 7.5), incubated for 1 h at 25 °C in 1% BSA–0.3% Triton X-100–TBS solution, and then kept at 4 °C in rabbit anti-c-Fos antibody (sc-52 LotG1108, Santa Cruz Biotechnology) solution (1:200 in 1% BSA-TBS). After TBS washing, sections were incubated for 1 h at 25 °C in Alexa Fluor 647-conjugated (Invitrogen) goat anti-rabbit secondary antibody (1:500 in 1% BSA-TBS).

Confocal microscopy and cell-counting. All brain slices were imaged by epifluorescence microscopy (Zeiss Imager M1) or confocal microscopy (Zeiss, LSM 800) for subsequent analysis. Brain areas were determined according to their anatomy using the Paxinos and Franklin brain atlas[54]. For PMv^{DAT} cell counts the entire PMv was cut, stained, and counted. Quantification of c-Fos staining

was obtained by averaging the number of positive cells of right and left PMv in two brain sections (–2.46 and –2.54 mm from bregma)[54]. All counts were done manually using ImageJ software and blind to test conditions.

Anterograde and retrograde tracing. Male mice injected unilaterally with AAV-DIO-ChR2-eYFP virus were perfused 5 weeks postinjection, and their brains were sectioned coronally (14-µm slices) and mounted on slides. Each brain area in which eYFP-immunoreactive fibers were detected was scanned by confocal microscope under uniform imaging settings (LSM 800, Zeiss, Germany). For retrograde tracing, male mice were injected bilaterally with Green Retrobeads (Lumafluor Inc.) and were perfused 2 weeks postinjection. The brains were sectioned into 14-µm coronal slices, and these were mounted on slides and analyzed under a fluorescence microscope to verify the injection site. Brain slices from the injection sites and PMv were imaged by confocal microscopy for further analysis of colocalization with the genetically expressed tdTomato-labeled PMv^{DAT} neurons containing green retrobeads.

Randomization and blinding. Behavioral data collection and analysis was performed blind to experimental conditions. Anatomy data analysis but not tissue collection was blinded. Electrophysiological data sampling and analysis were not blinded, with the exception of all whole-cell patch-clamp datasets presented in Fig. 1. Mice were first screened to determine whether they were AGG or NON and then randomly assigned to groups and further behavioral analysis.

Statistical analysis. No statistical methods were used to predetermine sample sizes, but our sample sizes are similar to those reported in previous publications[2,10,13,29,30]. Data met the assumptions of the statistical tests used and were tested for normality and equal variance. All *t* tests and one-way ANOVA were performed using Graph Pad Prism software (Graphpad Software Inc.). Tukey and Bonferroni post hoc tests were used as appropriate for one-way ANOVA. Normality was determined by D'Agostino–Pearson normality tests. Statistical significance was set at $P < 0.05$.

Reporting Summary. Further information on experimental design is available in the Nature Research Reporting Summary linked to this article.

Data availability statement. The data that support the findings of this study are available from the corresponding authors upon reasonable request.

References

50. Ekstrand, M. I. et al. Progressive Parkinsonism in mice with respiratory-chain-deficient dopamine neurons. *Proc. Natl. Acad. Sci. USA* **104**, 1325–1330 (2007).
51. Russo, S. J. et al. Nuclear factor kappa B signaling regulates neuronal morphology and cocaine reward. *J. Neurosci.* **29**, 3529–3537 (2009).
52. Petersson, U. et al. Nucleobindin is produced by bone cells and secreted into the osteoid, with a potential role as a modulator of matrix maturation. *Bone* **34**, 949–960 (2004).
53. Tulke, S. et al. Nucleobindin 1 (NUCB1) is a Golgi-resident marker of neurons. *Neuroscience* **314**, 179–188 (2016).
54. Franklin, K.B.J. & Paxinos, G. *The Mouse Brain in Stereotactic Coordinates*, 3rd ed. (Academic Press, Cambridge, MA, 2008).

nature research

Corresponding author(s): Stefanos Stagkourakis & Christian Broberger

Reporting Summary

Nature Research wishes to improve the reproducibility of the work that we publish. This form provides structure for consistency and transparency in reporting. For further information on Nature Research policies, see Authors & Referees and the Editorial Policy Checklist.

Statistical parameters

When statistical analyses are reported, confirm that the following items are present in the relevant location (e.g. figure legend, table legend, main text, or Methods section).

n/a	Confirmed	
☐	☒	The exact sample size (*n*) for each experimental group/condition, given as a discrete number and unit of measurement
☐	☒	An indication of whether measurements were taken from distinct samples or whether the same sample was measured repeatedly
☐	☒	The statistical test(s) used AND whether they are one- or two-sided *Only common tests should be described solely by name; describe more complex techniques in the Methods section.*
☐	☒	A description of all covariates tested
☐	☒	A description of any assumptions or corrections, such as tests of normality and adjustment for multiple comparisons
☐	☒	A full description of the statistics including central tendency (e.g. means) or other basic estimates (e.g. regression coefficient) AND variation (e.g. standard deviation) or associated estimates of uncertainty (e.g. confidence intervals)
☐	☒	For null hypothesis testing, the test statistic (e.g. *F*, *t*, *r*) with confidence intervals, effect sizes, degrees of freedom and *P* value noted *Give P values as exact values whenever suitable.*
☒	☐	For Bayesian analysis, information on the choice of priors and Markov chain Monte Carlo settings
☒	☐	For hierarchical and complex designs, identification of the appropriate level for tests and full reporting of outcomes
☐	☒	Estimates of effect sizes (e.g. Cohen's *d*, Pearson's *r*), indicating how they were calculated
☐	☒	Clearly defined error bars *State explicitly what error bars represent (e.g. SD, SE, CI)*

Our web collection on statistics for biologists may be useful.

Software and code

Policy information about availability of computer code

Data collection	In vitro electrophysiology data were collected in Clampex 10.8. Behavioural data were collected using IC capture cameras from imaging source, recording both top and side view. Confocal images were taken using the ZEN software from ZEISS.
Data analysis	In vitro electrophysiology data were analyzed in Clampfit 10.8, OriginPro 8.5 and Matlab using the signal processing toolbox. Behavioural data were scored with Ethovision XT 10. Statistical tests on data sets were performed with GraphPad Prism 6.

For manuscripts utilizing custom algorithms or software that are central to the research but not yet described in published literature, software must be made available to editors/reviewers upon request. We strongly encourage code deposition in a community repository (e.g. GitHub). See the Nature Research guidelines for submitting code & software for further information.

Data

Policy information about availability of data

All manuscripts must include a data availability statement. This statement should provide the following information, where applicable:

- Accession codes, unique identifiers, or web links for publicly available datasets
- A list of figures that have associated raw data
- A description of any restrictions on data availability

All materials used are readily available from standard commercial sources. Sources are specified in the method sections.

Field-specific reporting

Please select the best fit for your research. If you are not sure, read the appropriate sections before making your selection.

☒ Life sciences ☐ Behavioural & social sciences ☐ Ecological, evolutionary & environmental sciences

For a reference copy of the document with all sections, see nature.com/authors/policies/ReportingSummary-flat.pdf

Life sciences study design

All studies must disclose on these points even when the disclosure is negative.

Sample size	Sample sizes are estimated based on previous physiological studies using similar animal models to guarantee statistical relevance. Considering the typical variance of mouse social behaviour, we estimated that an n=10-20 animals per group allows for at least 80% statistical power when using the appropriate statistical test. Histological quantitative analyses was performed on similar group sizes to previous studies, typically with an n=10. Electrophysiological data for individual groups were collected from a minimum of n=3 mice. No further sample size calculation was performed.
Data exclusions	Animals injected with AAV and part of the behavioural optogenetics experiments, showing no detectable viral expression in the target region and/or ectopic fiber placement upon post-hoc histological examination were excluded from analysis. In electrophysiology whole-cell patch clamp recordings, access resistance was monitored throughout the experiments, and neurons in which the series resistance exceeded 15 MΩ or changed ≥20% were excluded from the statistics.
Replication	Behavioral experimental findings were reproduced in duplicates or triplicates and among individuals of a group. Electrophysiology and anatomy findings were replicable within groups.
Randomization	Randomization was performed in the majority of experimental designs in the current study. Randomization was performed during behavioral data collection. Male mice from the same litter were allocated in different experimental groups. Randomization was performed during electrophysiology data collection presented in Figure 1.
Blinding	Behavioural data collection and analysis was performed blind to experimental conditions. Anatomy data analysis but not tissue collection was blinded. Electrophysiological data sampling and analysis was not blinded, with the exception of all whole-cell patch clamp datasets presented in Figure 1.

Reporting for specific materials, systems and methods

Materials & experimental systems

n/a	Involved in the study
☐	☒ Unique biological materials
☐	☒ Antibodies
☒	☐ Eukaryotic cell lines
☒	☐ Palaeontology
☐	☒ Animals and other organisms
☒	☐ Human research participants

Methods

n/a	Involved in the study
☒	☐ ChIP-seq
☒	☐ Flow cytometry
☒	☐ MRI-based neuroimaging

Unique biological materials

Policy information about availability of materials

Obtaining unique materials	No restrictions on availability of reagents used in the present study apply.

Antibodies

Antibodies used	1. rabbit anti-NeuN (1:500; Cell Signalling, D4G40) 2. rabbit anti-NUCB1 (1:1,000; Dr M. Wendel lab; Petersson et al., 2004) 3. rabbit anti-c-fos antibody (1:200; sc-52 LotG1108, Santa Cruz Biotechnology) 4. chicken anti-GFP (1:500; Aves Labs, GFP-1020) 5. rabbit anti-ERα (1:200; Santa Cruz Biotechnology, sc-542) 6. rat anti-DAT (1:1000; Millipore, MAB369)

Validation

1. rabbit anti-NeuN (1:500; Cell Signalling, D4G40)
NeuN (D4G4O) XP® Rabbit mAb recognizes endogenous levels of total NeuN protein. This monoclonal antibody was produced by immunizing animals with recombinant protein specific to the amino terminus of human NeuN protein (RNA binding protein fox-1 homolog 3). PMID: 28848607, 28429775, 28423319, 27008987

2. rabbit anti-NUCB1 (1:1000; Dr M. Wendel lab)
The antibody was produced by immunizing rabbits with the peptide KVPEQPPELPQLDSQHL, corresponding to amino acids 439-455 in the C-terminal region of mouse NUCB1. Specificity of the antibody was validated by western blot and immunohistochemical analysis. PMID: 15193541, 26666627

3. Rabbit anti-c-fos antibody sc-52 LotG1108
This antibody was produced by immunizing rabbits with the N-terminus of c-Fos of human origin. The specificity of the AbI was validated in several mouse brain areas following open field ,object recognition and CPP test and in particular in the bilateral barrel field of the primary somatosensory cortex following whisker stimulation. In the last study, the specificity of the AbI was confirmed using another anti-c-Fos antibody (SC-253) that yielded similar results. PMID: 26136670, 25870909, 20463958

4. chicken anti-GFP (1:500; Aves Labs, GFP-1020)
Anti-GFP (Green Fluorescent Protein) was produced by immunization of chickens with purified recombinant green fluorescent protein (GFP) emulsified in Freund's adjuvant. The antibody was analyzed by western blot analysis and immunohistochemistry using transgenic mice expressing the GFP gene product. PMID: 28957379, 28885975, 28694334

5. rabbit anti-ERα
(1:200; Santa Cruz Biotechnology, sc-542) ERα Antibody (MC-20) is a rabbit polyclonal IgG recognizing the C-terminus of Estrogen receptor of mouse origin. PMID:29456719, 28938159, 28499383

6. rat anti-DAT (1:1000; Millipore, MAB369)
Rat were immunized with N-terminus of human dopamine transporter fused to Glutathione S-transferase. The AbI was validated in our and other laboratories as well by staining several mouse brain regions expressing DAT (i.e. Arcuate, ventral tegmental area, substantia nigra, Striatum, etc). Immunolocalization of DAT on sections of human brain using MAB369 shows dense punctate staining throughout the caudate, putamen and accumbens. DAT signal with this AbI is absent in the DAT-KO mouse and shows no cross reactivity to the closely related serotonin and norepinephrine transporters. PMID: 28417953, 29263318, 29038581, 28367951

Animals and other organisms

Policy information about studies involving animals; ARRIVE guidelines recommended for reporting animal research

Laboratory animals	Male C57BL/6J dopamine transporter (DAT)-Cre mice (Ekstrand et al., 2006) were used to genetically label and manipulate the DAT expressing neurons in the ventral premammillary nucleus. In addition to viral mediated labelling, to tag DAT+ PMv neurons DAT-Cre mice were crossed with Rosa26-lox-stop-lox-TdTomato (Ai14) reporter (The Jackson Laboratory stock 007905). Wild-type C57BL/6J (JAX mice strain) and BALB/c mice (BALB/cAnNCrl, strain code: 028, Charles River) were used in behavioural experiments.
Wild animals	No wild animals were used in the present study.
Field-collected samples	No field collected samples were used in the present study.